RAA 2019 Vol. **19** No. **8**, 121(20pp) doi: 10.1088/1674–4527/19/8/121

http://www.raa-journal.org *http://iopscience.iop.org/raa*

Research in Astronomy and Astrophysics

The local properties of supernova explosions and their host galaxies

Li Zhou[1,2,3], Yan-Chun Liang[2], Jun-Qiang Ge[2], Xu Shao[2], Xiao-Yan Chen[2] and Li-Cai Deng[2]

[1] Shandong Provincial Key Laboratory of Optical Astronomy and Solar-Terrestrial Environment, School of Space Science and Physics, Shandong University at Weihai, Weihai 264209, China
[2] National Astronomical Observatories, Chinese Academy of Sciences, Beijing 100101, China; *ycliang@nao.cas.cn*
[3] University of Chinese Academy of Sciences, Beijing 100049, China

Received 2019 June 7; accepted 2019 July 7

Abstract We aim to understand the properties at the locations of supernova (SN) explosions in their host galaxies and compare with the global properties of these host galaxies. We use the integral field spectrograph (IFS) of Mapping Nearby Galaxies at Apache Point Observatory (MaNGA) to generate 2D maps of the parameter properties for 11 SN host galaxies. The sample galaxies are analyzed one by one in detail in terms of their properties of velocity field, star formation rate, oxygen abundance, stellar mass, etc. This sample of SN host galaxies has redshifts around $z \sim 0.03$, which is higher than those of previous related works. The higher redshift distribution allows us to obtain the properties of more distant SN host galaxies. Metallicity (gas-phase oxygen abundance) estimated from integrated spectra can represent the local metallicity at SN explosion sites with small bias. All the host galaxies in our sample are metal-rich galaxies (12+$\log$(O/H)>8.5) except for NGC 6387, which means SNe may be more inclined to explode in metallicity-rich galaxies. There is a positive relation between global gas-phase oxygen abundance and the stellar mass of host galaxies. We also try to compare the differences of the host galaxies between SNe Ia and SNe II. In our sample, both SNe Ia and SNe II can explode in normal galaxies, but SNe II can also explode in an interacting or a merging system, in which star formation is occurring in the galaxy.

Key words: galaxies: abundances — galaxies: general — galaxies: stellar content — supernovae: general — techniques: spectroscopic

1 INTRODUCTION

Supernova (SN) explosions are one of the most important processes, which mark the end of a star's life. According to the presence or absence of various features in the spectra, SNe are classified into different types (Filippenko 1997). In the spectra of SNe I, hydrogen is absent. But in SNe II spectra, hydrogen is present. Among Type I SNe, the Si line is present in the spectra of SNe Ia, but the Si line is absent in the spectra of SNe Ib/c. The presence or absence of the He line distinguishes SNe Ib from SNe Ic (Hamuy et al. 2002; Turatto 2003). According to the light curves, SNe II can be classified into SNe IIP and IIL (Barbon et al. 1979). For the light curves of SNe IIP, there is a fast rise to peak (Rubin et al. 2016) followed by a long plateau ($\sim$90 d). For SNe IIL, the light curves present a fast rise to peak which is then followed by a linear decline (>1.4 mag/100 d). There are strong narrow or intermediate-width hydrogen emission lines superimposed on an otherwise smooth blue continuum in the spectra of SNe IIn (Schlegel 1990).

It is generally known that at the end of a star's life, which has initial mass larger than about 8 $M_\odot$, the star will explode due to gravitational collapse and leave a remnant of a neutron star or black hole (Bethe et al. 1979; Arnett et al. 1989). This is a core-collapse supernova (CCSN, including SN II and Ib/c). Becker & Iben (1980) showed that if the initial stellar mass of a star is less than 8 $M_\odot$, the star will explode to a degenerate carbon-oxygen (CO) white dwarf, which may be ignited when its mass increases to 1.4 $M_\odot$ due to accreting materials from its non-degenerate companion star, and it can be completely disrupted in a bright thermonuclear explosion that produces an SN Ia (Hoyle & Fowler 1960). SNe Ia are applied as standard candles to estimate distances in cosmology and they have led to the discovery of the accelerated expansion of the Universe and dark energy (Riess et al. 1998; Perlmutter et al. 1999).

The relations between different types of SNe and their host galaxies have been studied, such as in terms of luminosity, color and explosion environments of SNe, both on SNe Ia (Han et al. 2010) and CCSNe (Kelly & Kirshner 2012). Prieto et al. (2008) studied the metallicity of host galaxies with different types of SNe and found that SNe Ib/c tend to explode in galaxies with higher metallicity than SNe II. Shao et al. (2014) compared the properties of host galaxies for SN Ia, SN II and SN Ibc based on the Sloan Digital Sky Survey (SDSS) Data Release 7 (DR7), with 213 host galaxies as a working sample and 689 host galaxies as comparison ones. Data on the sample galaxies in these works are from fiber spectra.

Considering the different stellar populations of HII regions and clumps within one galaxy, an integral field spectrograph (IFS) targeting SN host galaxies is necessary to arrive at robust conclusions on the local environment of SNe and their progenitors. An IFS allows the combination of spatial and specific spectral information on the local SNe explosion sites and other sites in the host galaxies, and simultaneously to enable investigating the properties of SN progenitors. Thanks to improvements and integral field unit (IFU) spectroscopic surveys with modern telescopes, some works have made this possible and focused their studies on the local environment or progenitors of SNe.

With the wide-field IFU spectrograph PMAS/PPAK at the 3.5 m telescope of Calar Alto Observatory, Stanishev et al. (2012) compared the properties of seven nearby Type Ia SN explosion sites with those of their host galaxies. Kuncarayakti et al. (2013a) presented their investigation of 11 SNe Ib/Ic explosion sites on the IFS observations obtained using the SuperNova Integral Field Spectrograph (SNIFS) mounted at the University of Hawaii 2.2 m telescope (UH88) and the Gemini Multi-Object Spectrograph (GMOS) with the 8.1 m Gemini North telescope at Mauna Kea. Kuncarayakti et al. (2013b) performed a similar study of 13 SNe II-P and II-L explosion sites in nearby galaxies. Galbany et al. (2016a) conducted an analysis of the local explosion environments of 11 SNe that exploded in six nearby galaxies ($z \leq 0.016$), which were observed by the Multi-Unit Spectroscopy Explorer (MUSE) on the Very Large Telescope (VLT).

To obtain a more complete statistical analysis on hosts of different types of SNe, several researches have enlarged the sample of SN host galaxies. Based on the Calar Alto Legacy Integral Field Area (CALIFA), the PPAK IFS Nearby Galaxies Survey (PINGS) and some other observations, Galbany et al. (2014) analyzed IFU spectroscopy of 81 galaxies that hosted 95 SNe with different types. Galbany et al. (2016b) further extended SN host galaxies and analyzed the metallicity of 115 SN host galaxies. With the PMAS/PPak Integral-field Supernova hosts COmpilation (PISCO), Galbany et al. (2018) presented the properties of a sample of SN hosts with an IFS, which included 232 galaxies that hosted 272 SNe. Kuncarayakti et al. (2018) explored and analyzed 83 nearby CCSN explosion sites with an IFS. Lyman et al. (2018) performed spectroscopic environmental measurements for a sample of 37 SNe Iax (a peculiar SN class and different from normal SNe Ia) and their host galaxies using both IFS and long-slit data from VLT/MUSE and Nordic Optical Telescope/Andalucia Faint Object Spectrograph and Camera (NOT/ALFOSC).

The Mapping Nearby Galaxies at Apache Point Observatory (MaNGA, Bundy et al. 2015) should make an important contribution to understanding the properties of SN host galaxies, especially at the SN explosion sites, both on the individual target with detailed analyses and on the statistical properties based on a larger sample of host galaxies through exploration of different types of SNe. Chen et al. (2017) and Izzo et al. (2018) investigated one especially nearby superluminous supernova (SLSN) 2017egm using MaNGA IFU data and provided detailed analysis of the nearby environment of this SN. It is necessary to analyze a larger sample size in detail.

In this paper, we will examine detailed properties of 11 SN host galaxies (four Type Ia, five Type II and two unclassified types) by using their IFS observations from MaNGA. We will compare the properties in the region of SN explosion sites with those of the global regions for these host galaxies, regarding the properties of star formation rates (SFRs), gas-phase oxygen abundances, stellar masses, stellar population ages, etc. Most of our sample of galaxies have redshift around 0.03 following the selection of MaNGA sample galaxies. This redshift value is higher than the SN host galaxies in other works which normally have median value of redshift around 0.01. We will specially discuss this in Section 5.1. We will extend our sample size from the MaNGA database and try to make a statistical conclusion on the properties of SN host galaxies in the following work.

The paper is organized as follows: In Section 2, we present the method that is used to select our sample. The data reduction of IFU observation is described in Section 3. The properties of environment for different types of SNe are listed in Section 4. Finally, we discuss our results in Section 5 and draw conclusions in Section 6. Throughout this paper, we adopt a cosmological model with $H_0 = 70\,\mathrm{km\,s^{-1}\,Mpc^{-1}}$, $\Omega_M = 0.3$ and $\Omega_\Lambda = 0.7$.

2 SAMPLE SELECTION

To select the SN host galaxies within the field of view (FoV) of MaNGA, we match the Asiago Supernova

Catalog (ASC) with 1390 IFU galaxies from the first MaNGA public data release, which is part of SDSS Data Release 13 (DR13, Albareti et al. 2017). The details of cross-correlation will be described as follows.

2.1 Asiago Supernova Catalog

ASC was initially developed by Barbon et al. (1984), which contained some basic information about 568 SNe and host galaxies scrutinized from the year 1885 to 1983. The total number of 661 SNe and host galaxies discovered before 1988 December 31 was listed in Barbon et al. (1989). Ten years later, Barbon et al. (1999) presented data on a larger number of 1447 SNe and host galaxies. The Asiago SN group has been updating continually and has presented 6530 SNe and their host galaxies discovered before 2016 January 1.

Compared with the Sternberg Astronomical Institute (SAI) Supernova Catalogue, which was last modified on 2014 October 17, ASC has been updated more recently, so it presents a larger number of SNe and has more exact information about SNe and their host galaxies. Meanwhile, ASC includes two decimal places for right ascension (R.A.) and declination (Dec.) of SN coordinates.

2.2 MaNGA Survey

The SDSS-IV/MaNGA survey is designed to map 10 000 nearby galaxies and is intended to help clarify the process associated with galaxies from their birth and growth to finally their death (Weijmans & MaNGA Team 2016; Bundy et al. 2015; Law et al. 2015; Drory et al. 2015; Blanton et al. 2017). To elucidate this process, MaNGA will make good use of the SDSS-III BOSS spectrograph (Smee et al. 2013) to generate 2D spectrograph maps. Moreover, the spectra of MaNGA could characterize the internal composition and dynamical state of a sample of 10 000 galaxies, whose stellar masses are greater than $10^9\ M_\odot$.

The MaNGA sample is intended to have both Primary and Secondary samples, which should cover more than 1.5 R_e and 2.5 R_e, respectively. The median redshift of the Primary and Secondary samples is 0.03 and 0.045, respectively (see Bundy et al. 2015; Law et al. 2015; Wake et al. 2017; Yan et al. 2016 in more detail). Law et al. (2015) found that the best IFU shape is a regular hexagonal form, and it realized 3 μm root mean square (rms) fiber placement using MaNGA hardware. We can produce 2D maps of many parameters from MaNGA, including Hα velocity, gas-phase oxygen abundance, SFR, stellar mass, etc., to trace the formation and evolution processes of galaxies.

2.3 Cross-correlations of Catalogs and Final Sample

To study the local properties of SNe and their host galaxies, we cross-correlate the R.A. and Dec. of 6530 SNe from ASC displayed up to 2015 December 31 with the R.A. and Dec. of 1390 galaxies from MaNGA in SDSS DR13. The largest diameter of the IFU is 32″, so here we adopt 15″ as the matching radius. There are 14 sample galaxies selected. There are 3 out of 14 SN host galaxies excluded: 2 of 14 SNe cannot be examined in the FoV of MaNGA, and the signal to noise ratio (S/N) for 1 of 14 SN host galaxies is too low to be analyzed. Finally, we select 11 galaxies in this matching radius that have been observed. The reason why the sample ratio in this work is smaller than that in Galbany et al. (2016b) in the CALIFA sample will be discussed in Section 5.1.

Figure 1 shows the range of redshift and absolute magnitude in the r band (M_r, which is from MaNGA) of our sample galaxies and DR13 MaNGA galaxies marked by grey dots. There is a gap for DR13 MaNGA galaxies, which results from the sample selection of MaNGA (Primary and Secondary Samples, e.g., Wake 2015; Belfiore et al. 2016). From this figure, the M_r of 11 galaxies ranges from –23 to –19 mag, and the redshifts are mostly around 0.03 but with one having 0.008 and another having 0.0789. Details of our 11 sample galaxies are presented in Table 1. From Table 1, we can see that there are four SNe Ia, five SNe II and two unclassified types of SNe in our sample. The host galaxies of SN 2004eb (Type II, NGC 6387) and 1999gw (unclassified type, UGC 04881NED02) are in a merging system. In particular for SN 1999gw, the interaction region is inside the FoV of MaNGA.

3 DATA ANALYSIS

3.1 IFS Analysis

We go through three steps from MaNGA data cube to galaxy emission line measurements and then use the emission line measurements to obtain the parameters of galaxies, such as gas abundance, SFR, etc.

3.1.1 Voronoi 2D binning

Considering that the spectral S/Ns are usually less than 1 at the edge of the MaNGA FoV, we therefore spatially rebin those spaxels with low S/N together to improve the spectral S/N, which allow us to obtain reliable spectral fitting results. For each spectrum, its S/N is defined as the median S/N of the whole spectrum, which is dominated by the continuum, instead of those regions at the blue or red end, or those emission lines.

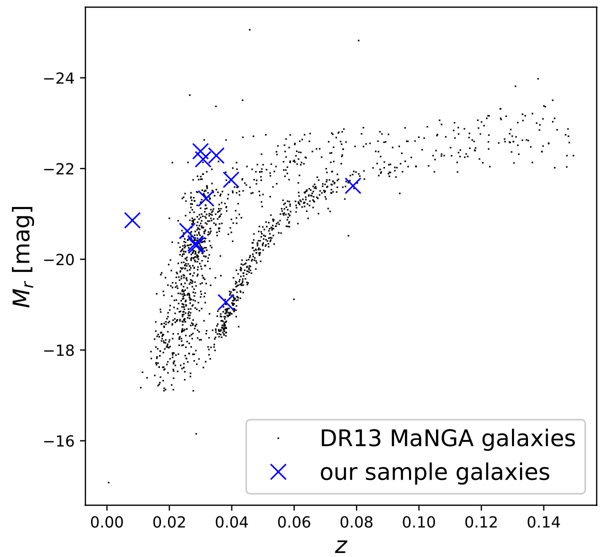

Fig. 1 The redshift and absolute magnitude in r band distributions of all the 11 sample galaxies compared with the DR13 MaNGA sample galaxies.

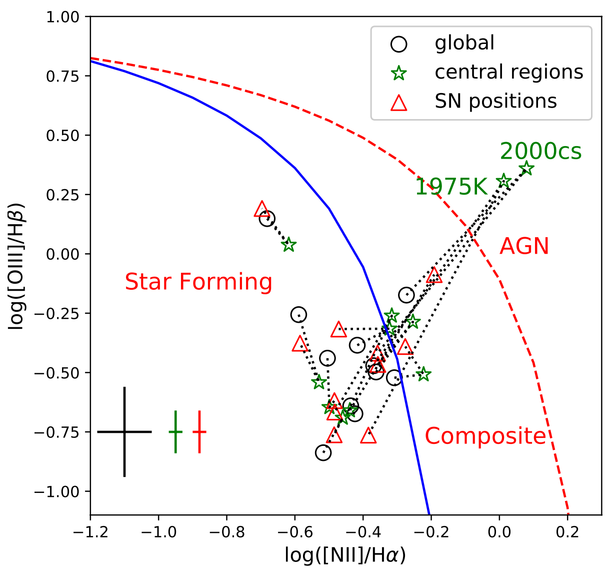

Fig. 2 The BPT diagram of the sample galaxies. We plot the emission-line flux ratio of log([O III]/Hβ) versus the ratio log([N II]/Hα) for all the galaxies in our sample. The errorbars are the average standard deviation of the log([O III]/Hβ) and log([N II]/Hα) for the global SN host galaxies (*black circles*), central regions of SN host galaxies (*green stars*) and the explosion sites (*red triangles*).

Here we apply the Voronoi 2D binning method (Cappellari & Copin 2003) to perform the spatial rebinning, and set the rebinned spectra to have S/N=20, which guarantees relatively high spatial resolution for our science and high enough S/N for reliable spectral analysis. Before the binning, those spectra with S/N< 3 are removed due to their small contribution to the spectral S/N improvement.

3.1.2 *Stellar population synthesis*

In this work, we apply the `STARLIGHT` code (Cid Fernandes et al. 2005) and the simple stellar population (SSP) library from the Bruzual & Charlot (2003) (BC03) model with Chabrier initial mass function (Chabrier 2003) to perform the spectral fitting and stellar population analysis. For the SSP library, the selected SSP templates include 24 different ages and six different metallicities as follows:

– The stellar ages: [0.001, 0.003, 0.005, 0.007, 0.009, 0.01, 0.014, 0.025, 0.04, 0.055, 0.1, 0.16, 0.29, 0.51, 0.9, 1.28, 1.43, 2.5, 4.25, 6.25, 7.5, 10.0, 13.0, 15.0] Gyr;
– The metallicities ($Z/Z_\odot$): [0.005, 0.02, 0.2, 0.4, 1.0, 2.5].

The current selection on age and metallicity grids allows us to fit both the late and early types of galaxies with different metal abundances.

We resample all the spectra with $\Delta\lambda = 1\,\text{Å}$ linearly before the `STARLIGHT` fitting. In the spectral fitting, we assume the Calzetti law (Calzetti et al. 2000) for dust extinction correction, and set the parameter A_V as free. Taking into account the uncertainties of flux calibration, we allow a negative A_V in each spectral fitting. Following the suggestions from Cid Fernandes et al. (2005), we deredshift each spectrum to rest-frame wavelength. During the spectral fitting, we only take the spectra with wavelength ranging from 3700 Å to 7000 Å which includes those emission lines from [O II]3727 to [S II]6731.

After the `STARLIGHT` fitting, 99% of the spectra in our sample have $A_V < 1$. In this case, the derived stellar population parameters are reliable and have no significant biases (Ge et al. 2018; Cid Fernandes 2018). Therefore, for the current sample, we can use the `STARLIGHT` code for both stellar population analysis and emission-line measurements.

3.1.3 *Emission-line measurements*

As was described in the SDSS spectral fitting paper (Ge et al. 2012), after the `STARLIGHT` fitting, we resample the model spectra with 1 Å to the observed spectral resolution. We get the resampled model spectra with continuum and absorption lines subtracted and finally obtain the pure-emission-line spectra. Errors of the data points in the pure-emission-line spectra are taken as the same as those in the MaNGA data cube. In the case of weak emission lines, whether the continuum of pure-emission-line spectra is zero will strongly affect the emission-line fitting. We use a linear fit to adjust the shape of the continuum, then treat each emission line as a Gaussian with three parameters: line width, flux and offset (with respect to the rest-

Table 1 Basic Information from MaNGA and ASC about Our 11 Sample Galaxies

Plate IFU	SN name	SN type	SN R.A.	SN Dec.	Host	Type	Redshift	b/a	PA	Kinematics[e]
8261–12705	2007sw	Ia	183.4037	46.4934	UGC 7228	Sbc[b]	0.0257	0.41	179.9	RD
7975–6104	2006iq	Ia	324.8906	10.4849	PGC 1380172	Sb[d]	0.0789	0.87	79.2	RD
8138–12704	2007R	Ia	116.6564	44.7895	PGC 21767	S0/a[b]	0.0308	0.69	14.9	RD
8332–1902	2005cc	Ia pec	209.2702	41.8449	NGC 5383	SBb[b]	0.00814	0.70	62.8	RD
8604–12701	2000cs	II pec	245.8843	39.1248	MCG +07-34-015	Sb[d]	0.0350	0.98	21.0	RD
7495–12702	2010ee	II	205.0750	26.3533	UGC 8652	Sb[d]	0.0284	0.29	165.5	RD
8453–12702	2012al	IIn	151.5485	47.2946	PGC 213664	Sb[d]	0.0381	0.55	12.7	RD
8588–6101	2011cc	IIn	248.4560	39.2635	IC 4612	Sc[c]	0.0318	0.96	18.9	RD
7990–3703	2004eb	II	262.1013	57.5460	NGC 6387	Sb[d]	0.0286	0.62	92.1	PR
8250–12704	1999gw	U[a]	138.9779	44.3319	UGC 4881	Interaction [c]	0.0398	0.63	108.9	CK
8550–12705	1975K	U[a]	249.1371	39.0301	NGC 6195	Sb[b]	0.0300	0.67	141.4	RD

Notes: [a] unclassified; [b] based on ASC; [c] based on SDSS pseudo-images; [d] based on Dobrycheva (2013); [e] based on Yang et al. (2008) and Hammer et al. (2017). RD: rotating disk; PR: perturbed rotation; CK: complex kinematics.

Table 2 The Values of $\log([\text{N II}]/\text{H}\alpha)$ and $\log([\text{O III}]/\text{H}\beta)$ Estimated from Global Galaxy Spectra, Central and SN Positions

SN	SN type	Host	$\log([\text{N II}]/\text{H}\alpha)$			$\log([\text{O III}]/\text{H}\beta)$		
			Global	Center	Local	Global	Center	Local
2007sw	Ia	UGC 7228	–0.50±0.07	–0.50±0.02	–0.48±0.02	–0.44±0.18	–0.65±0.09	–0.62±0.10
2006iq	Ia	PGC 1380172	–0.42±0.07	–0.44±0.03	–0.19±0.01	–0.67±0.18	–0.66±0.05	–0.09±0.11
2007R	Ia	PGC 21767	–0.44±0.08	–0.32±0.05	–0.48±0.02	–0.64±0.19	–0.26±0.11	–0.67±0.04
2005cc	Ia pec	NGC 5383	–0.52±0.05	–0.46±0.02	–0.48±0.01	–0.84±0.11	–0.69±0.05	–0.76±0.06
2000cs	II pec	MCG +07-34-015	-0.27±0.14	0.08±0.03	–0.36±0.02	–0.17±0.26	0.36±0.07	–0.42±0.07
2010ee	II	UGC 8652	–0.42±0.08	–0.32±0.02	–0.47±0.03	–0.38±0.26	–0.32±0.04	–0.32±0.14
2012al	IIn	PGC 213664	–0.59±0.07	–0.53±0.02	–0.59±0.05	–0.26±0.17	–0.54±0.10	–0.38±0.15
2011cc	IIn	IC 4612	–0.36±0.07	–0.25±0.05	–0.36±0.05	–0.50±0.21	–0.29±0.11	–0.47±0.12
2004eb	II	NGC 6387	–0.68±0.08	–0.20±0.01	–0.70±0.04	0.15±0.09	0.04±0.01	0.19±0.09
1999gw	U	UGC 4881	–0.31±0.14	–0.22±0.05	–0.28±0.05	–0.52±0.23	–0.51±0.12	–0.39±0.09
1975K	U	NGC 6195	–0.37±0.10	0.01±0.02	–0.38±0.02	–0.47±0.23	0.31±0.13	–0.76±0.07

Table 3 The values of global SFR for a galaxy (SFR_g), the global sSFR of the host galaxies and the local sSFR at the SN explosion sites, gas extinction at SN position (A_{Vl}) and global stellar mass of the host galaxies.

SN	SN type	Host	SFR_g ($M_\odot\,\text{yr}^{-1}$)	$\log(\text{sSFR}_g)$ (yr^{-1})	$\log(\text{sSFR}_l)$ (yr^{-1})	A_{Vl} (mag)	$\log(M/M_\odot)$[a] STARLIGHT	$\log(M/M_\odot)$[b] DRP	$\log(M/M_\odot)$[c] MPA/JHU
2007sw	Ia	UGC 7228	3.42±0.003	–9.96±0.001	–10.00±0.001	1.84±0.01	10.49	10.34	...
2006iq	Ia	PGC 1380172	3.41± 0.029	–10.32±0.004	–10.78±0.116	1.84±0.40	10.85	10.73	10.96
2007R	Ia	PGC 21767	4.45±0.026	–10.34±0.003	–10.22±0.003	1.70±0.02	10.99	11.00	11.16
2005cc	Ia pec	NGC 5383	0.53±0.005	–9.98±0.004	–9.74±0.008	1.71±0.05	9.7	10.40	7.50
2000cs	II pec	MCG +07-34-015	0.32±0.013	–11.15±0.018	–11.37±0.171	0.98±1.29	10.6	11.06	11.08
2010ee	II	UGC 8652	1.18±0.011	–10.42±0.004	–10.39±0.004	1.11±0.09	10.49	10.28	10.61
2012al	IIn	PGC 213664	0.04±0.002	–10.99±0.026	–11.04±0.026	0.96±0.48	9.55	9.56	9.60
2011cc	IIn	IC 4612	4.30±0.008	–10.00±0.001	–9.99±0.001	0.97±0.06	10.63	10.56	10.74
2004eb	II	NGC 6387	5.62±0.038	–8.97±0.003	–9.22±0.005	0.40±0.08	9.72	9.61	9.61
1999gw	U	UGC 4881	13.04±0.138	–9.93±0.005	–10.12± 0.026	1.98±0.15	11.05	10.73	10.95
1975K	U	NGC 6195	2.26±0.082	–10.56±0.016	–10.26±0.015	1.38±0.18	10.91	11.05	11.17

[a] The global stellar mass of the host galaxies estimated using the STARLIGHT code in this work;
[b] The global stellar mass of the host galaxies taken from the DRP catalog (Law et al. 2016);
[c] The global stellar mass of the host galaxies taken from MPA/JHU (Kauffmann et al. 2003a; Salim et al. 2007).

frame central wavelength). To measure these weak emission lines more accurately, we fix the offset and width of all emission lines but with flux free. We also imposed two flux ratio constraints: [O III] λ5007/[O III] λ4959=2.97 and [N II] λ6583/[N III] λ6548=3.

3.2 Emission Line Fluxes and Extinction

With the above emission line fitting, we can derive emission-line fluxes of Hα, Hβ, [O III] λ5007, [N II] λ6583, [O II] λ3727 and [S II] $\lambda\lambda$6716/6731. To perform a robust analysis on the emission line related results (e.g., gas metallicity), we then exclude those spaxels that have low S/N (< 3). For instance, to estimate the gas-phase oxygen abundance using the O3N2 method (Pettini & Pagel 2004), only those spaxels that have their emission lines of Hα, Hβ, [O III] λ5007 and [N II] λ6583 measured with S/N>3 simultaneously are included to calculate the metallicity.

The emission line fluxes are corrected for dust extinction in the direction of line of sight through galaxies, which could be estimated by Hα and Hβ emission lines (Osterbrock & Ferland 2006). In the case of B recombination, the ratio of I(Hα) and I(Hβ) is 2.86, and the electron density and electron temperature are $10^2\,\mathrm{cm}^{-3}$ and 10 000 K, respectively (Osterbrock & Ferland 2006). Applying the equation $R_V = A_V/E(B-V)$ provided by Fitzpatrick (1999) and the value of $R_V = 3.1$, we compute A_V. We can estimate the gas velocity field from the strong Hα emission lines using the method of Krajnović et al. (2006). Then the position angle (PA) and redshift of the host galaxies can be derived.

3.3 Star Formation Rate

We estimate the ongoing SFR from Hα luminosity according to the relation given by Kennicutt (1998)

$$\mathrm{SFR}[M_\odot \mathrm{yr}^{-1}] = 7.9 \times 10^{-42} L(\mathrm{H}\alpha), \tag{1}$$

where $L(\mathrm{H}\alpha)=4\pi d_L^2 F(\mathrm{H}\alpha)$, which is H$\alpha$ luminosity in units of $\mathrm{erg\,s^{-1}}$, d_L is the luminosity distance to the galaxy in units of cm and F(Hα) is the extinction-corrected flux of Hα in $\mathrm{erg\,s^{-1}\,cm^{-2}}$. Given 2D maps of properties of galaxies, there are two methods to measure global ongoing SFR: summing the SFR of all the single spaxels in the FoV of MaNGA and estimating from the Hα emission line flux of the global spectra in the FoV of MaNGA. The results of these two methods agree well for the spaxels with high S/N. Here we use the first one to estimate the global SFR of SN host galaxies. Also, we estimate the specific star formation rate (sSFR) as SFR/M, where M is the relevant mass estimated from the `STARLIGHT` code. We generate 2D maps of sSFR to show the distributions.

3.4 Gas-phase Oxygen Abundance

There are several methods to estimate the oxygen abundance. The most straightforward approach is the electron temperature method (Te method). It is often estimated from [O III] λ5007, [O III] λ4959/[O III] λ4363 (e.g., Stasińska 2006; Izotov et al. 2006; Liang et al. 2006, 2007). However, we should notice that the most important and temperature sensitive emission line [O III] λ4363 is difficult to measure, especially in a metal-rich environment (Izotov et al. 2006). All of our sample galaxies do not have a strong [O III] λ4363 line. Therefore, we have to employ other strong line methods to estimate oxygen abundance, like the O3N2, N2O2 and R_{23} methods.

R_{23} is one of the most commonly used methods (Pilyugin & Thuan 2005; Pagel et al. 1979; McGaugh 1991; Zaritsky et al. 1994; Tremonti et al. 2004; Kewley & Dopita 2002; Kobulnicky & Kewley 2004; Pilyugin 2001)

$$\begin{aligned}\mathrm{R}_{23} =&(I_{[\mathrm{O\,II}]\lambda3727} + I_{[\mathrm{O\,III}]\lambda4959} \\ &+ I_{[\mathrm{O\,III}]\lambda5007})/\mathrm{H}\beta.\end{aligned} \tag{2}$$

It has a special feature, which sometimes is also a severe shortcoming in that metallicity increases with increasing R_{23} in the metal-poor branch, but decreases in the metal-rich branch. So, the key problem with R_{23} is to choose the real relation to avoid double peaks. Here we apply the relation in Tremonti et al. (2004) to estimate the gas-phase oxygen abundance

$$\begin{aligned}12+\log(\mathrm{O/H}) =&9.185 - 0.313 \times \log(\mathrm{R}_{23}) \\ &- 0.24 \times (\log(\mathrm{R}_{23}))^2 \\ &- 0.321 \times (\log(\mathrm{R}_{23}))^3.\end{aligned} \tag{3}$$

This relation is only suitable for galaxies with a metal-rich environment (12 + log(O/H) $>$ 8.5).

In this work, we also use the O3N2 and N2O2 methods. Alloin et al. (1979) defined O3N2

$$\mathrm{O3N2} = \log(([\mathrm{O\,III}]\lambda5007/\mathrm{H}\beta)/([\mathrm{N\,II}]\lambda6583/\mathrm{H}\alpha)). \tag{4}$$

Pettini & Pagel (2004) showed that there is an apparent and significant linear relation between O3N2 and log(O/H) when the value of O3N2 is located in the region between –1 and 1.9

$$12+\log(\mathrm{O/H}) = 8.73 - 0.32 \times \mathrm{O3N2}\,. \tag{5}$$

Liang et al. (2006) used a sample ($8.4 \leq 12+\log(\mathrm{O/H}) \leq 9.3$, $-1.2 \leq \log([\mathrm{N\,II}]/[\mathrm{O\,II}]) \leq 0.7$) from SDSS to acquire the linear relation

$$\mathrm{N2O2} = \log(([\mathrm{N\,II}]\lambda6583)/([\mathrm{O\,II}]\lambda3727))\,, \tag{6}$$

$$12+\log(\mathrm{O/H}) = 9.125 + 0.49 \times \mathrm{N2O2}\,. \tag{7}$$

Compared with other methods, Zhang et al. (2017) indicated that metallicities estimated employing the N2O2 method have the smallest bias and error for Diffuse Ionized Gas (DIG) and HII regions. According to Zhang et al. (2017), the N2O2 method can only be affected by the N/O abundance ratio and temperature, but it is not subject to ionization parameter or variation in ionizing spectrum shape (Dopita et al. 2000, 2013). The key problem for this method is that dust extinction should be corrected accurately.

4 RESULTS

From emission line fluxes, we obtain dust extinction, SFR, oxygen abundance, stellar mass and stellar population age. Figure 2 presents the Baldwin, Phillips and Terlevich (BPT, Baldwin et al. 1981) diagram for our sample galaxies. The values of emission line flux ratios and parameters are presented from Table 2 to Table 5. The 2D maps of the properties for the host galaxies of four Type Ia, five Type II and two unclassified types of SNe are shown in Figures 3, 4 and 5, respectively. The global values of parameters are estimated using all the useful spaxels of the host galaxies in the FoV of MaNGA. We take a circular region with 4″ diameter around the host galaxy centers and the SNe positions to estimate the values of parameters at the central regions and SN locations, respectively. Here we should note that for SN 1999gw, which exploded in a merging system, the global values of parameters are estimated using all useful spaxels of the system in the FoV of MaNGA.

4.1 BPT Diagnostic Diagram

When estimating the gas-phase oxygen abundance, active galactic nuclei (AGNs) should be excluded from calculation and analysis since the existence of AGNs somewhat biases the measurements. To distinguish AGN contamination from star-forming regions in the centers of galaxies, we adopt the BPT diagram, which can separate emission line galaxies from AGNs according to different excitation mechanisms (Baldwin et al. 1981). Figure 2 shows the BPT diagram of our sample. The horizontal axis is the value of $\log$([N II] λ6583/Hα) and the vertical axis represents the value of $\log$([O III] λ5007/Hβ). The dashed line traces the boundary between AGNs and composite galaxies and it is taken from Kewley et al. (2001). The blue solid line separates composite galaxies from star-forming galaxies and it is adopted from Kauffmann et al. (2003b). The hollow circles, green stars and red triangles represent the positions of the global galaxy spectrum, the galaxy nuclei and the SN locations, respectively. For every single sample galaxy, these three points are connected using dotted lines. The average standard deviation of $\log$([N II] λ6583/Hα) and $\log$([O III] λ5007/Hβ) for the global SN host galaxies, central regions of SN host galaxies and SN explosion sites are about 0.08 and 0.19, 0.02 and 0.09, and 0.02 and 0.09 dex, respectively. The errorbars are marked in the left corner of the BPT diagram.

The values of emission line flux ratios of the global, central regions and SNe explosion regions are presented in Table 2. According to Figure 2 and Table 2, the centers of the host galaxy for the unclassified type of SN 1975K (NGC 6195) and the host galaxy of SN II 2000cs (MCG +07–34–015) are in the AGN regions. However, their global spectra are located in the star-forming galaxies and composites regions. We can infer that for these two galaxies, the effect of AGNs is too small to change the global galaxy spectra (Stanishev et al. 2012). The difference of the emission line ratio in Figure 2 between SN location and global spectrum is a little larger for SNe 2006iq, 2007sw and 1975K. The global spectrum for the host galaxy of SN 2006iq (PGC 1380172) is located in the star forming region, while the SN 2006iq is located in the composite region. For the other sample galaxies, the difference in the emission line ratio between local and global cases is small.

4.2 Hα Velocity Field

The Hα velocity distributions are displayed in the 2D maps. With the method of analysis from Krajnović et al. (2006), we can distinguish whether the galaxy is pure disk rotation or not, which is shown in Table 1.

For distant galaxies, a simple kinematic classification was developed based on the 3D kinematics and morphology by Flores et al. (2006). Yang et al. (2008) and Hammer et al. (2017) summarized the differences between different classes. For rotating disks (RDs), the velocity field presents an ordered gradient and the dynamical major axis is consistent with the morphological major axis. There is a single peak in the velocity dispersion (σ) map, which is located close to the dynamical center. The features of the velocity field of perturbed rotations (PRs) are similar to an RD, but there is no peak or the peak is apparently shifted away from the dynamical center in the σ map. For complex kinematics (CK), both the velocity field distribution and the σ map are irregular and not compatible with regular disk rotation. This classification is based on the large-scale structure of distant galaxies (Hammer et al. 2017). Therefore, we can roughly classify our host galaxies into RD, PR and CK as marked in Table 1.

According to Figure 3, the Hα velocity gradient of the host galaxies for all the four Type Ia SNe 2007sw (UGC 7228), 2006iq (PGC 1380172), 2007R (PGC 21767) and 2005cc (NGC 5383) are smooth without irregularities. There are some spaxels that have a higher σ in the host galaxies and they are distributed in the outer regions of the FoV. We infer that this may be caused by the low S/N for the spaxels in the outer region. Roughly, the host galaxies of all the SNe Ia only have one peak in σ and the peaks are located at the centers of the host galaxies. Therefore, all the SNe Ia host galaxies here are almost RD. That is to say, in our four sample galaxies, SNe Ia explode in normal galaxies without turbulence.

According to Figure 4, the Hα velocity gradients of the host galaxies of all the five Type II SNe have al-

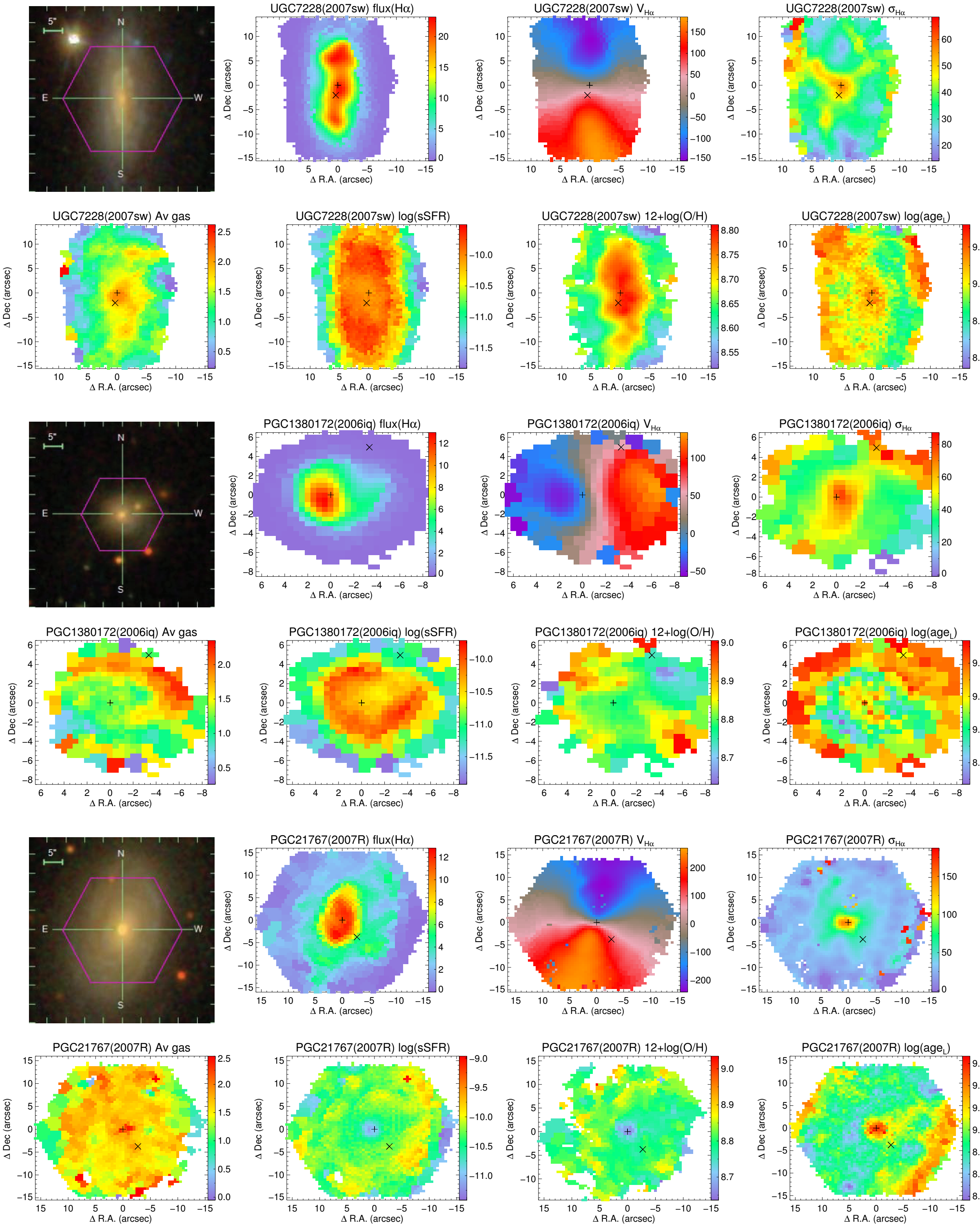

Fig. 3 The 2D maps of SN Ia host galaxies, including Hα flux in units of erg s^{-1} cm^{-2}, Hα velocity in units of km s^{-1}, velocity dispersion in units of km s^{-1}, gas and dust extinction in units of mag, sSFR in units of yr^{-1}, oxygen abundance estimated using the O3N2 method and the logarithm of light-weighted stellar age estimated using `STARLIGHT` in units of log[yr]. The coordinates in the X and Y axes are in units of arcsec with respect to the 2D map centers. In each panel, the plus marks the position of the galaxy center and the cross signifies the location of the SN. There is only one spaxel left by limiting the S/N≥3 for the SN 2006iq explosion site in the host galaxy. So, we do not cut spaxels with S/N≤3 in the metallicity 2D map for this SN host galaxy.

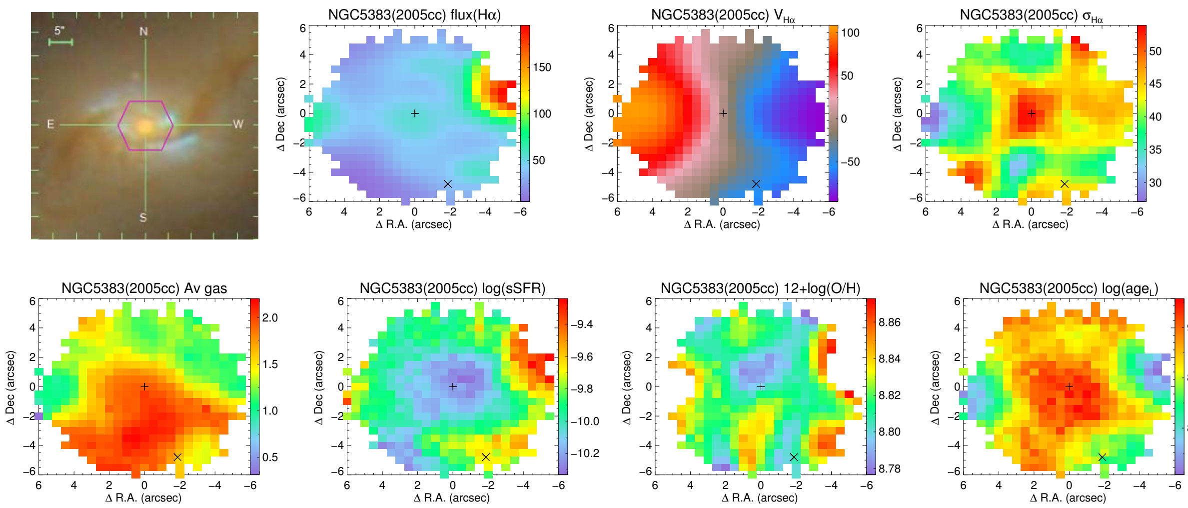

Fig. 3 —*Continued.*

Table 4 The gas-phase oxygen abundance estimated from global galaxy spectra, the central regions of SN host galaxies and SN positions using O3N2, N2O2 and R_{23} methods.

SN	SN type	Host	O3N2_PP04			N2O2			R_{23}		
			12+log(O/H)$_g$ [a]	12+log(O/H)$_c$ [b]	12+log(O/H)$_l$ [c]	12+log(O/H)$_g$ [a]	12+log(O/H)$_c$ [b]	12+log(O/H)$_l$ [c]	12+log(O/H)$_g$ [a]	12+log(O/H)$_c$ [b]	12+log(O/H)$_l$ [c]
2007sw	Ia	UGC 7228	8.65 ± 0.13	8.78 ± 0.03	8.78 ± 0.04	8.88 ± 0.13	8.95 ± 0.03	8.98 ± 0.05	8.90 ± 0.14	9.01 ± 0.04	9.02 ± 0.06
2006iq[d]	Ia	PGC 1380172	8.72 ± 0.18	8.80 ± 0.03	8.66 ± 0.19	9.02 ± 0.16	9.11 ± 0.04	9.01 ± 0.20	9.02 ± 0.16	9.14 ± 0.03	8.98 ± 0.20
2007R	Ia	PGC 21767	8.77 ± 0.12	8.73 ± 0.07	8.78 ± 0.09	9.06 ± 0.13	9.01 ± 0.09	9.06 ± 0.08	9.08 ± 0.13	8.85 ± 0.13	9.10 ± 0.06
2005cc	Ia pec	NGC 5383	8.82 ± 0.04	8.82 ± 0.02	8.81 ± 0.06	9.08 ± 0.05	9.09 ± 0.03	9.07 ± 0.05	9.12 ± 0.05	9.13 ± 0.02	9.12 ± 0.04
2000cs	II pec	MCG +07-34-015	8.68 ± 0.18	...	8.66 ± 0.20	9.04 ± 0.18	...	9.04 ± 0.20	9.04 ± 0.18	...	9.05 ± 0.19
2010ee	II	UGC 8652	8.67 ± 0.15	8.71 ± 0.04	8.70 ± 0.11	8.93 ± 0.15	8.97 ± 0.07	8.94 ± 0.12	8.92 ± 0.17	8.85 ± 0.12	8.95 ± 0.13
2012al	IIn	PGC 213664	8.58 ± 0.18	8.67 ± 0.17	8.58 ± 0.18	8.87 ± 0.18	8.90 ± 0.17	8.86 ± 0.16	8.91 ± 0.18	8.95 ± 0.18	8.90 ± 0.17
2011cc	IIn	IC 4612	8.73 ± 0.12	8.75 ± 0.02	8.76 ± 0.04	8.99 ± 0.13	9.03 ± 0.03	9.04 ± 0.05	8.93 ± 0.15	8.93 ± 0.07	8.99 ± 0.09
2004eb	II	NGC 6387	8.43 ± 0.07	8.52 ± 0.02	8.48 ± 0.15	8.73 ± 0.07	8.81 ± 0.02	8.75 ± 0.12	8.68 ± 0.09	8.78 ± 0.03	8.73 ± 0.15
1999gw	U	UGC 4881	8.75 ± 0.13	8.79 ± 0.08	8.77 ± 0.07	8.97 ± 0.14	8.97 ± 0.08	8.89 ± 0.08	8.90 ± 0.17	8.91 ± 0.11	8.71 ± 0.11
1975K	U	NGC 6195	8.72 ± 0.16	...	8.85 ± 0.06	8.99 ± 0.17	...	9.09 ± 0.06	9.00 ± 0.17	...	9.10 ± 0.05

[a] Global gas-phase oxygen abundance of the host galaxies;

[b] The gas-phase oxygen abundance of the central regions of the host galaxies. No measurements because the galaxies harbor AGNs in their centers;

[c] Local gas-phase oxygen abundance of SN explosion sites;

[d] As explained in the caption of Fig. 3, we do not cut the spaxels with S/N≤3 when estimating the metallicity for this SN host galaxy.

most regular Hα velocity distribution. For SN 2004eb, there is more than one peak in the σ map of the host galaxy (NGC 6387), which indicates that the host galaxy of SN 2004eb (NGC 6387) is PR. It can also be shown from the images of MaNGA that NGC 6387 is in an interacting system. However, for the other four Type II SN host galaxies, there is only one peak in the σ map and the peak is located at the centers of galaxies, which signifies that these host galaxies are RD. Four out of five SNe II host galaxies in our sample are RD, and one is PR, which indicate that for our sample galaxies SNe II tend to explode in normal galaxies or an interacting or merging system.

According to Figure 5, the Hα velocity gradient of the host galaxy of unclassified type of SN 1975K (NGC 6195) is smooth without irregularities. The σ map has only one peak in the galaxy center. Therefore, according to the velocity field and the σ map, NGC 6195 is almost RD without turbulence. While for the host galaxy of SN 1999gw (UGC 4881), the Hα velocity distribution is irregular. From the maps of σ, the host galaxy of SN 1999gw (UGC 4881) has more than one peak, so there is turbulence in this galaxy. Therefore, according to the classification criteria in Yang et al. (2008), the kinematic type of UGC 4881 is CK, which can also be shown from the image of MaNGA that this galaxy is in a merging system.

4.3 Hα Flux, Extinction and Star Formation Rate

We estimate SFR through Hα flux, which has been corrected for dust extinction. Here we classify our sample into three groups (galaxies that host SNe Ia, galaxies that host SNe II and galaxies that host unclassified type of supernovae) and analyze them below in three groups.

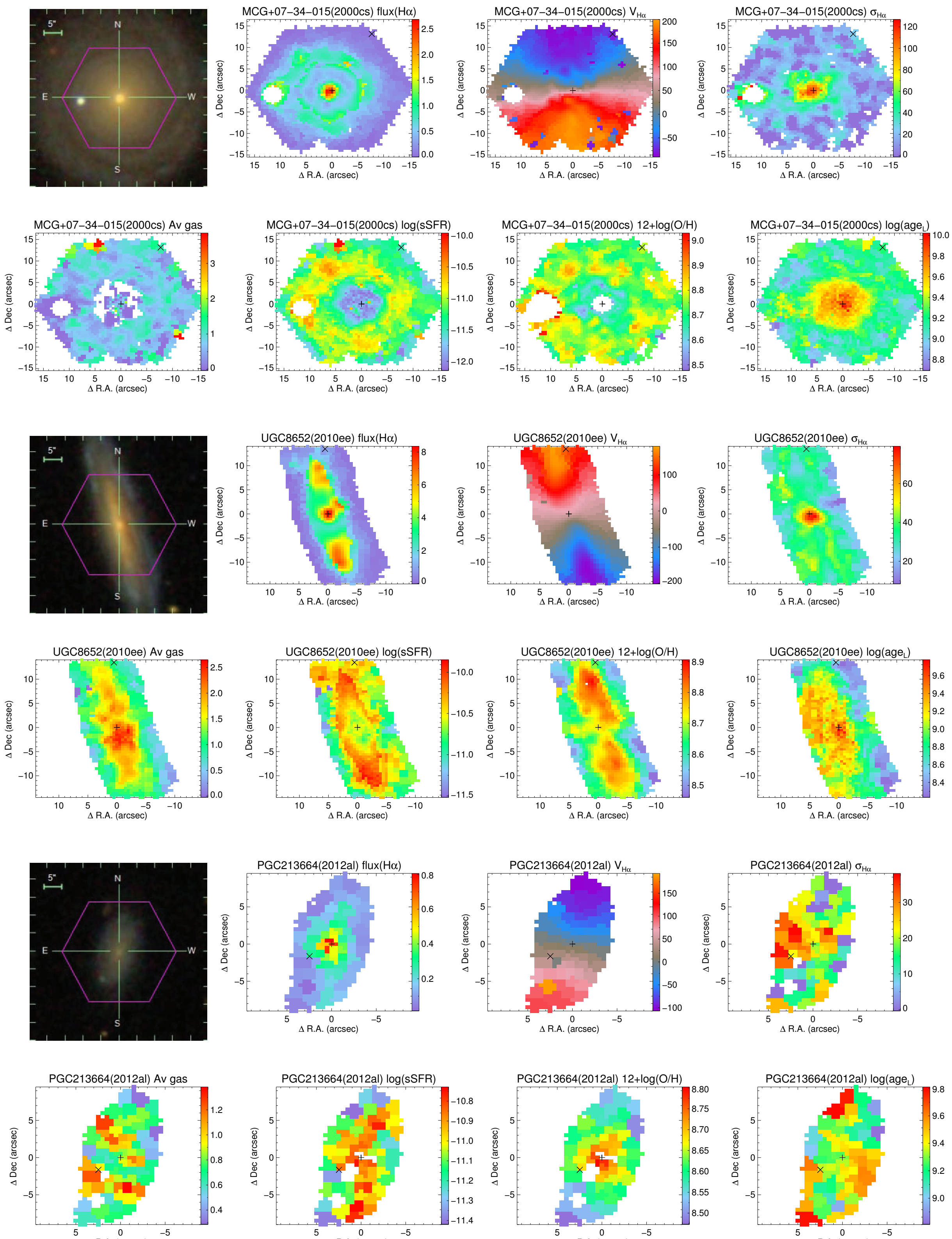

Fig. 4 Same as Fig. 3, but for SN II host galaxies. There are only several spaxels left by limiting the S/N≥3 for the SN 2000cs explosion site in the host galaxy. So, we do not cut spaxels with S/N≤3 in the sSFR and metallicity 2D maps for this SN host galaxy.

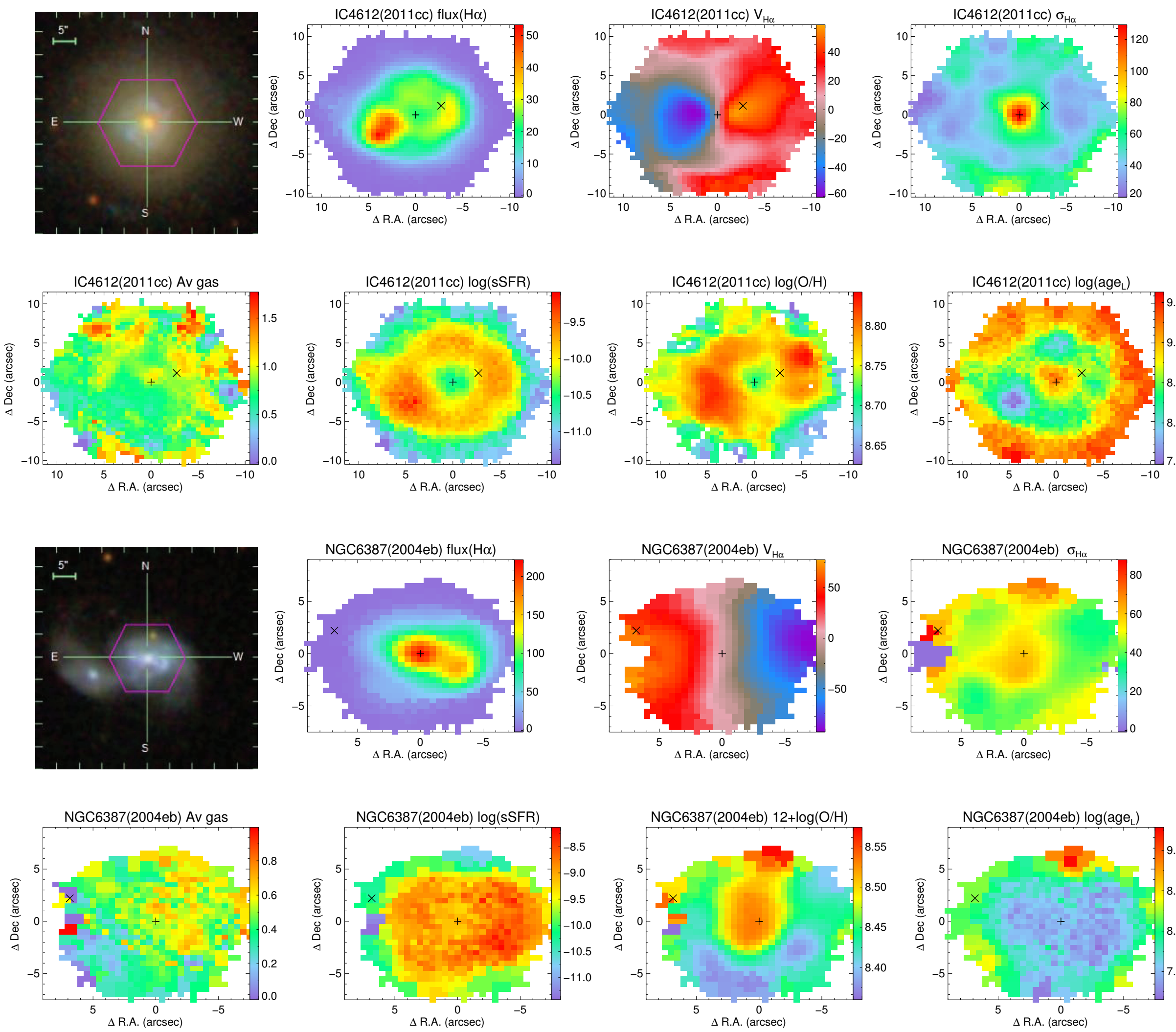

Fig. 4 —*Continued.*

4.3.1 SNe Ia

UGC 7228, PGC 1380172, PGC 21767 and NGC 5383 are host galaxies of Type Ia SNe 2007sw, 2006iq, 2007R and 2005cc, respectively.

From Figure 3, we can see that the Hα flux of these four galaxies has the highest value in the center except for the host galaxy of SN 2005cc (NGC 5383). According to James et al. (2009), there is an obvious Hα flux deficit in the center of late-type spirals (Sc+), but a very different behavior in Sa-type spirals such that the Hα flux increases towards the center. James et al. (2009) demonstrate that the Hα flux radial distribution of unbarred Sb spirals is similar to that of Sa spirals, but Hα flux of barred Sb spirals is strong in the center, then it decreases before Hα flux increases again. According to ASC and Dobrycheva (2013), the types of host galaxies for SNe Ia 2007sw, 2006iq, 2007R and 2005cc belong to Sbc, SB, S0/a and SBb, respectively. The morphology of the host galaxies is consistent with classification from the Hα flux distribution of the images provided by MaNGA based on the classification method in James et al. (2009).

Table 3 shows the global SFR of host galaxies in units of $M_\odot$ yr^{-1}, the global sSFR of the host galaxies and the local sSFR at the SNe explosion sites in units of yr^{-1} and gas extinction at SN position (A_{Vl}) in units of mag.

Stanishev et al. (2012) mentioned that in their sample galaxies, the extinction would increase with the Hα flux, which was explained in that extinction was expected to be observed in the star formation regions. From the 2D maps of our Figure 3, we can see that the gas and dust extinction distribution is not always the same as the trend of Hα flux in our sample galaxies, especially for the host galaxy of SN 2005cc (NGC 5383). The extinctions A_{Vl} of the four Type Ia SNe positions are high, up to about 1.84, which are given in Table 3.

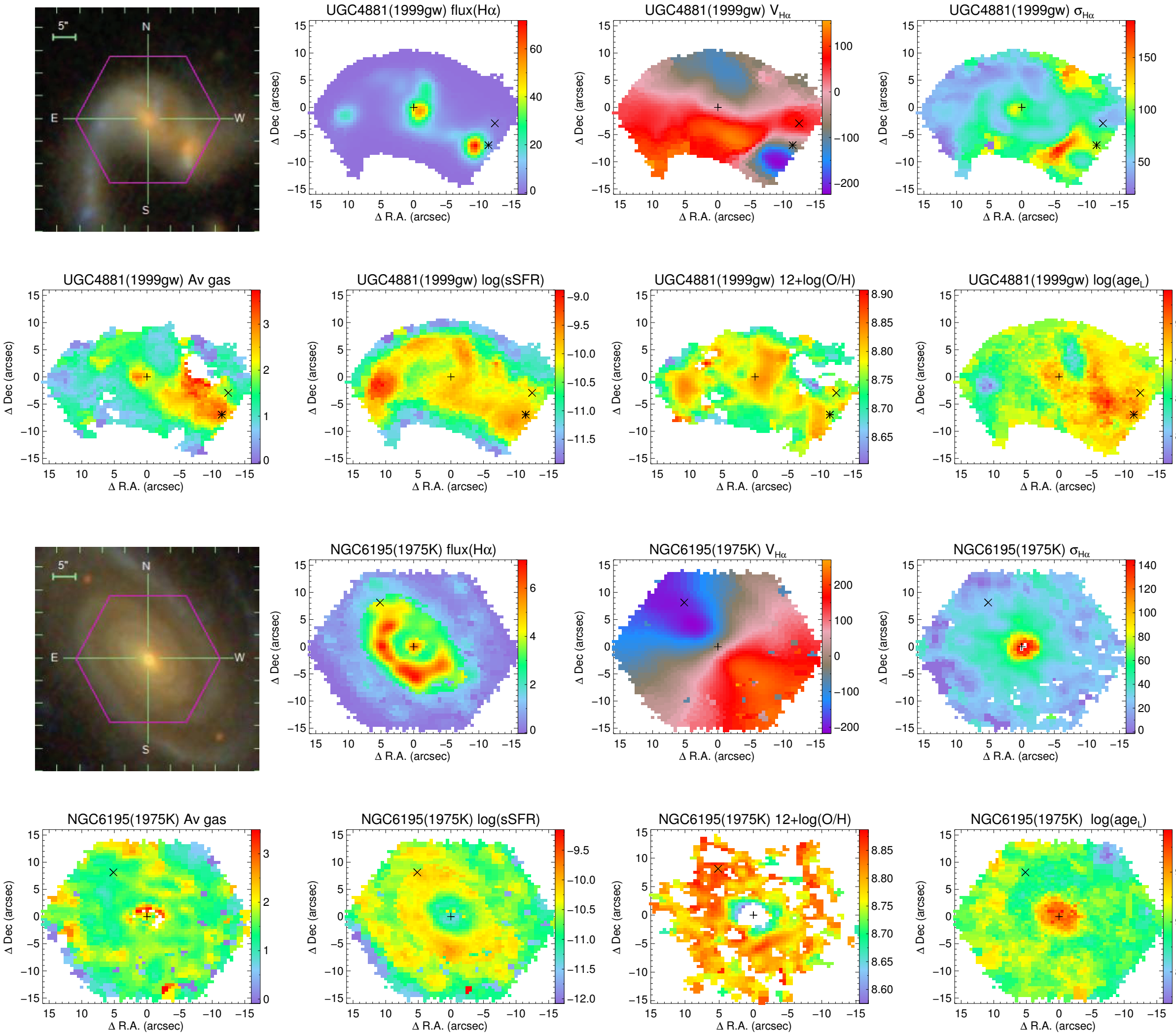

Fig. 5 Same as Fig. 3 but for unclassified SN host galaxies. For the host galaxy of SN 1999gw, in each panel, a *plus* marks the center of the FoV of the merging system, and a *cross* signifies the center of the other galaxy in the merging system, the real SN host of 1999gw (UGC 4881 NED02).

Table 5 The mass-weighted and light-weighted stellar population age estimated from global galaxy spectra and SN positions, and the fractions of spaxels in the range of stellar population age. This also presents the global and central values of Dn(4000) and Hδ_A for the sample galaxies.

SN	SN type	Host	$age_{M,g}$ (log[yr])	$age_{M,l}$ (log[yr])	$age_{L,g}$ (log[yr])	$age_{L,l}$ (log[yr])	$age_{L,young}$ fraction	$age_{L,int}$ fraction	$age_{L,old}$ fraction	Dn(4000)$_g$	H$\delta_{A,g}$ (Å)	Dn(4000)$_c$	H$\delta_{A,c}$ (Å)
2007sw	Ia	UGC 7228	9.79 ± 0.13	9.92 ± 0.08	9.01 ± 0.28	9.26 ± 0.12	1.79	88.03	10.18	1.39 ± 0.05	5.03 ± 0.82	1.47 ± 0.01	4.21 ± 0.20
2006iq	Ia	PGC 1380172	9.79 ± 0.15	9.73 ± 0.20	9.22 ± 0.17	9.35 ± 0.10	0.00	80.50	19.50	1.53 ± 0.26	3.20 ± 1.38	1.54 ± 0.03	2.81 ± 0.28
2007R	Ia	PGC 21767	9.85 ± 0.11	9.87 ± 0.05	8.95 ± 0.21	8.98 ± 0.08	0.25	96.36	3.39	1.51 ± 0.10	3.22 ± 0.90	1.84 ± 0.05	-0.32 ± 0.42
2005cc	Ia pec	NGC 5383	9.89 ± 0.12	9.82 ± 0.13	8.64 ± 0.34	8.44 ± 0.14	27.25	72.75	0.00	1.37 ± 0.08	4.61 ± 1.01	1.53 ± 0.03	2.68 ± 0.39
2000cs	II pec	MCG +07-34-015	9.75 ± 0.17	9.72 ± 0.13	9.23 ± 0.20	9.18 ± 0.06	0.00	80.07	19.93	1.57 ± 0.14	2.59 ± 1.57	2.02 ± 0.03	-1.27 ± 0.17
2010ee	II	UGC 8652	9.75 ± 0.17	9.60 ± 0.18	8.93 ± 0.34	8.52 ± 0.20	13.14	79.97	6.89	1.41 ± 0.11	4.79 ± 1.33	1.68 ± 0.04	1.37 ± 0.30
2012al	IIn	PGC 213664	9.92 ± 0.14	9.98 ± 0.11	9.36 ± 0.23	9.39 ± 0.16	0.00	52.10	47.90	1.34 ± 0.06	5.24 ± 0.97	1.45 ± 0.02	4.04 ± 0.23
2011cc	IIn	IC 4612	9.66 ± 0.13	9.82 ± 0.07	8.82 ± 0.40	8.63 ± 0.16	20.94	73.99	5.07	1.43 ± 0.11	3.78 ± 1.33	1.56 ± 0.05	1.57 ± 0.32
2004eb	II	NGC 6387	9.11 ± 0.39	8.97 ± 0.18	7.82 ± 0.37	8.05 ± 0.17	95.90	4.10	0.00	1.20 ± 0.05	5.43 ± 0.82	1.19 ± 0.01	5.15 ± 0.14
1999gw	U	UGC 4881	9.64 ± 0.30	9.81 ± 0.15	8.92 ± 0.30	9.17 ± 0.14	6.54	88.03	5.43	1.40 ± 0.08	5.66 ± 0.99	1.45 ± 0.03	3.57 ± 0.32
1975K	U	NGC 6195	9.79 ± 0.11	9.78 ± 0.09	9.01 ± 0.19	8.97 ± 0.10	0.98	95.07	3.95	1.50 ± 0.09	3.70 ± 1.22	1.93 ± 0.03	-0.79 ± 0.29

young: $age_L \leq 300$ Myr; intermediate: 300 Myr $< age_L <$ 2.4 Gyr; old: $age_L \geq$ 2.4 Gyr.

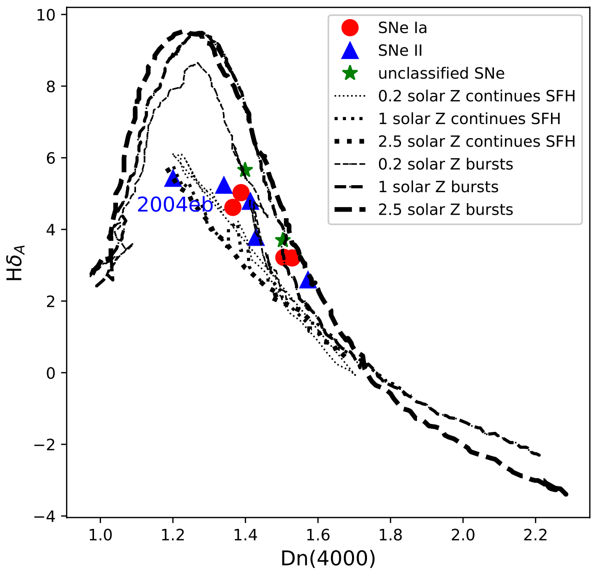

Fig. 6 The distribution of global Dn(4000) and Hδ_A for our SN galaxies. The *dashed lines* are the relations between Dn(4000) and Hδ_A for 20 per cent solar, solar and 2.5 times solar metallicity bursts. The *dotted lines* are the relations between Dn(4000) and Hδ_A for 20 per cent solar, solar and 2.5 solar metallicity continuous star formation histories. These lines are from Kauffmann et al. (2003a).

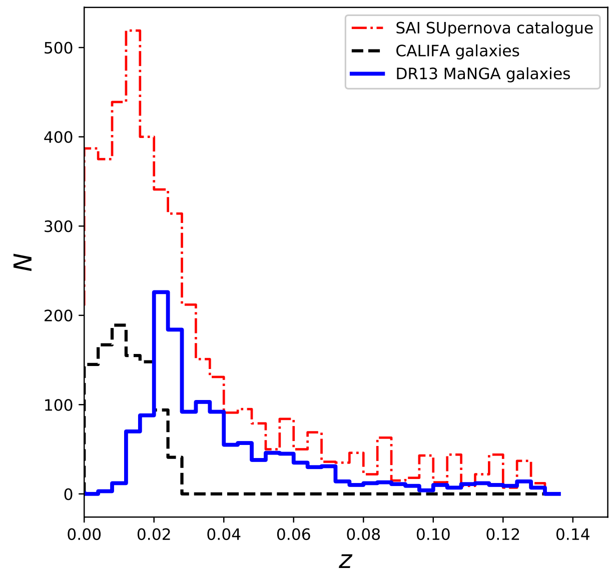

Fig. 7 The histogram distribution of redshift for galaxies from the SAI Supernova Catalogue, CALIFA and MaNGA galaxies in SDSS DR13.

Compared with the global sSFR of SN Ia host galaxies, the local sSFR at the SN explosion sites is similar or higher for SNe 2007sw, 2007R and 2005cc, which exploded close to the centers of their host galaxies. While for SN 2006iq, which exploded in the outer region of its galaxy center, the local sSFR at the SN explosion site is lower than the global sSFR for the host galaxy. Figure 3 also displays the 2D maps of sSFR for SNe Ia host galaxies. From this figure, sSFR decreases towards outer regions for SNe 2007sw and 2006iq, while SNe 2007R and 2005cc have a lower sSFR in the centers of their host galaxies than those in the outer regions. Also, the figures and Table 3 indicate that the SN positions are close to the highest sSFR region except for SN 2006iq, which exploded in the outer region that has much lower sSFR than the global value.

4.3.2 SNe II

From Figure 4, the host galaxies of Type II SN 2000cs (MCG +07-34-015), 2010ee (UGC 8652), 2012al (PGC 213664) and 2004eb (NGC 6387) have the highest Hα flux in the center in each galaxy, which indicates that these galaxies are unbarred Sb-type spiral galaxies. From the pseudo-color image of MaNGA, the host galaxy of 2004eb (NGC 6387) is in the process of merging, which will affect the SFR, oxygen abundance, etc. The SN 2004eb is on the edge of the FoV of this galaxy. The host galaxy of SN 2011cc (IC 4612) has an Hα flux deficit in

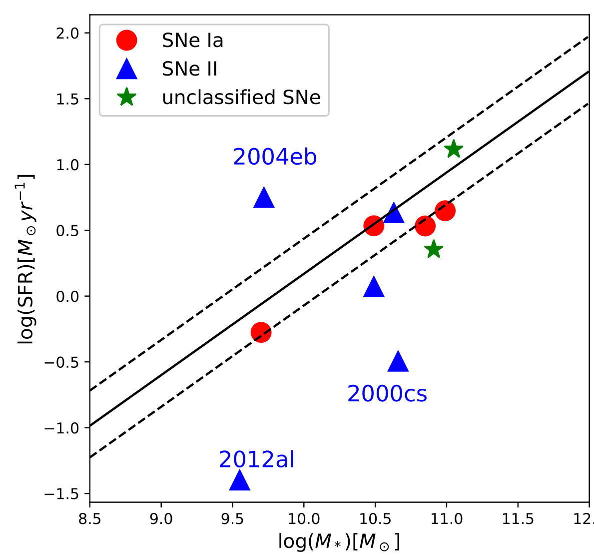

Fig. 8 The relation between global SFR and stellar mass estimated using the STARLIGHT code. The blue SDSS galaxies at $0.015 \leq z \leq 0.1$ follow the relation (*solid line*): SFR[$M_\odot$ yr^{-1}]= 8.7[–3.7, +7.4] × ($M_\star$ / 10^{11} $M_\odot$)$^{0.77}$ at the 68% confidence level (*dashed lines*, Elbaz et al. 2007). The *red circles*, *blue triangles* and *green stars* represent SNe Ia, SNe II and unclassified type of SNe, respectively.

the center, and the SN is located at the ring of the host galaxy.

From Figure 4, we can see that the gas and dust extinction distribution of Type II SN 2010ee host galaxy increases towards the center, and displays a similar trend as the Hα flux. However, according to the image and the inclination, the host of SN 2010ee is an edge-on galaxy, so it is difficult to estimate the extinction accurately. For the other four Type II SN host galaxies, the trend of dust extinction is not always the same as the Hα flux. The local dust extinctions of the five Type II SNe explosion sites are lower than those of SNe Ia.

Figure 4 also shows 2D maps of sSFR for the five Type II SN host galaxies. SNe 2000cs and 2004eb are on the edge of the FoV of hosts and have lower sSFR at the SNe positions than those of global values of host galaxies, which are also shown in Table 3. The sSFRs at the SN positions of SNe 2010ee, 2012al and 2011cc are almost the same as the global value.

4.3.3 Unclassified type of supernovae

The local dust extinctions of these two SN explosion sites are higher than those of SNe II, as can be ascertained in Table 3. From the pseudo-color image of MaNGA and Hα flux 2D map, we can see that the host galaxy of SN 1999gw (UGC 4881) is in a merging system. The host galaxy of SN 1975K (NGC 6195) is an Sb-type spiral galaxy based on the morphology type in ASC, which also can be seen from the MaNGA image.

Figure 5 depicts the 2D maps of the sSFR for these two unclassified types of SN host galaxies. According to Figure 5, SN 1999gw exploded close to the region that has the highest Hα flux, but the Hα flux at the specific SN explosion site is much lower. There are double peaks in the sSFR distribution for the host galaxy of SN 1999gw (UGC 4881) apparent in Figure 5, which is consistent with the morphology of the merging system. From Table 3, the sSFR at the SN position of SN 1999gw is lower than the global value. SN 1975K is located in the region where Hα flux is lower than the center, but higher than the outer regions. From Table 3, the sSFR at the SN position of SN 1975K is higher than the global value of the host galaxy NGC 6195. Figure 5 demonstrates that it has the highest value of sSFR in the spiral arm regions of the galaxy and the sSFR of the central region of the galaxy is lower.

4.4 Gas Phase Oxygen Abundances

Gas-phase oxygen abundance distributions estimated by the O3N2 method of Pettini & Pagel (2004) in 2D maps are displayed from Figure 3 to Figure 5 for our sample galaxies. The global gas-phase oxygen abundance of the host galaxies and local value at SN explosion sites estimated by O3N2, N2O2 and R_{23} methods are listed in Table 4. According to the BPT diagram, the emission line ratios of the centers of SNe 2000cs and 1975K host galaxies are located in the regions of AGNs. Even though the effect of AGNs is small, the central regions of these two host galaxies, MCG +07-34-015 and NGC 6195, which harbor AGNs in their centers, are masked in the process of calculating oxygen abundance. The existence of AGNs will bias the global spectra and cause deviation when estimating the gas-phase oxygen abundance. Also, emission lines with S/N less than 3 are masked to reduce computational errors.

4.4.1 SNe Ia

Figure 3 shows 2D maps of gas-phase oxygen abundance of four SN Ia host galaxies. The oxygen abundance increases towards the center of the host galaxy of 2007sw (UGC 7228), which indicates an inside to outside formation of the galaxy. In the center, the metalliciy reaches the highest value and the SN 2007sw is located close to the highest metallicity. The oxygen abundances decrease towards the central regions for the host galaxies of SNe Ia 2006iq (PGC 1380172) and 2007R (PGC 21767), which means an outside to inside formation of the galaxies. The host galaxy of 2007R (PGC 21767) has been analyzed in Stanishev et al. (2012). Our result for this galaxy agrees well with Stanishev et al. (2012). The host galaxy of 2005cc (NGC 5383) shows an irregular distribution of metallicity. There is a spindly region which presents apparently lower metallicity and is believed to be where the spiral arm is located.

Table 4 lists the metallicity estimated from the global galaxy spectra, central regions and SN locations using the O3N2, N2O2 and R_{23} methods. From Table 4, we can see that the local gas-phase oxygen abundance at the SN 2007sw explosion site is higher than the global value. For SN 2006iq, the local oxygen abundance is lower than the global value. The local oxygen abundances at the SN explosion sites of SNe 2007R and 2005cc are nearly the same as those of the global value for their host galaxies.

4.4.2 SNe II

For the five Type II SNe, Figure 4 presents the 2D maps of gas-phase oxygen abundance. We can see from the 2D map of the host galaxy of 2000cs (MCG +07-34-015) that the center is masked due to the presence of an AGN, and the metallicity increases in the outer regions. There are two peaks of gas-phase oxygen abundance in the host galaxy of 2010ee (UGC 8652), which may be in the spiral arms, but the center has lower metallicity. The gas phase oxygen abundances of host galaxies of SN 2012al (PGC 213664) and 2004eb (NGC 6387) increase towards the centers. SN 2011cc is located close to the region that has the highest metallicity. The metallicity of the host galaxy of SN 2011cc (IC 4612) increases from the center, and decreases after running up to the peaks. We suppose that the peaks are on the ring of the host galaxy.

From Table 4, the local oxygen abundance is almost the same as the global value estimated by the O3N2, N2O2 and R_{23} methods for SNe 2000cs, 2010ee, 2012al, 2011cc and 2004eb.

4.4.3 Unclassified type of supernova

The host galaxy of SN 1999gw (UGC 4881) is in a merging system. The 2D map of the gas-phase oxygen abundance in this merging system is fan-shaped. Figure 5 shows that there are double peaks of gas-phase oxygen abundance, one is in the central regions of the FoV of MaNGA (UGC 4881 NED01, marked by pluses), and the other is located at the right bottom of the field (UGC 4881 NED02, marked by crosses). The SN 1999gw is located close to the peak. From Table 4, the difference between local gas-phase oxygen abundance estimated by the O3N2 method of SN 1999gw and the global value of host galaxy UGC 4881 is small. According to Figure 5, the gas phase oxygen abundance of SN 1975K's host galaxy decreases from outside towards the central regions. From Table 4, we can see that the local gas phase oxygen abundance of SN 1975K is a little higher than that of the global value.

4.5 Stellar Mass

In this work, we estimate the current stellar mass using `STARLIGHT` fits (Cid Fernandes et al. 2005). The global stellar masses of SN host galaxies are shown in Table 3. For comparison, we have also given the stellar mass taken from the MaNGA Data Reduction Pipeline (DRP) catalog (Law et al. 2016), and the total stellar mass of SN galaxies taken from MPA/JHU (Kauffmann et al. 2003a; Salim et al. 2007) in Table 3. There are no stellar mass data for the SN 2007sw host galaxy (UGC 7228) in MPA/JHU. The difference between these three stellar masses calculated using three different methods is very small except for the host galaxy of SN 2005cc (NGC 5383). The stellar mass of this galaxy is $10^{9.7}\,M_\odot$ as calculated by `STARLIGHT`, $10^{10.4}\,M_\odot$ taken from DRP (Law et al. 2016) and $10^{7.5}\,M_\odot$ taken from MPA/JHU. The FoV of MaNGA bundles only cover the inside $1.5\,R_e$ or $2.5\,R_e$ of the galaxy, so we cannot derive the whole galaxy mass based on the IFU data. The galaxy stellar mass given by DRP is based on photometry data, which are calculated by using the photometry image of the whole galaxy and can hence provide us the mass of the whole galaxy. The masses from MPA/JHU are measured from a single fiber spectrum of the nucleus, scaled to the photometry of the whole galaxy, which may bias the final result because it assumes the same stellar populations and L/M along the galaxy. The lower mass of NGC 5383 from MPA/JHU may mainly result from the wrong photometry.

Here we should note that the calculated stellar mass for SN 1999gw's host galaxy is for the merging system, including the host galaxies UGC 4881 NED02 and UGC 4881 NED01.

4.6 Stellar Age

We estimate stellar age using `STARLIGHT` fits. The 2D maps of light-weighted stellar age of the SN galaxies are presented from Figure 3 to Figure 5.

Cid Fernandes et al. (2005) pointed out that this value is very uncertain for the individual components of the stellar population vectors estimated by `STARLIGHT`. The scatter of the measurements estimated from every single pixel is too large to derive the authentic rules. The scatter increases as the galactocentric distance increases, which is caused by low S/N in the outer region of the galaxy. Following Cid Fernandes et al. (2005), to provide a more robust description of the current stellar population of the galaxies, Stanishev et al. (2012) presented a roughly binned version of the stellar population ranges, which divide the stellar populations: young stellar population range ($\mathrm{age}_L \leq 300\,\mathrm{Myr}$), intermediate stellar population range ($300\,\mathrm{Myr} < \mathrm{age}_L < 2.4\,\mathrm{Gyr}$) and old stellar population range ($\mathrm{age}_L \geq 2.4\,\mathrm{Gyr}$).

We provide the global mass-weighted and light-weighted stellar population ages for the host galaxies and the local SNe explosion sites, and the fractions of spaxels in the bins of young, intermediate and old stellar populations in Table 5. From Table 5, the light-weighted stellar population ages are lower than the mass-weighted ones. The light-weighted age has a higher weight for the younger stellar population. In our sample galaxies, the mean mass-weighted stellar population age is more than $10^{9.5}$ yr except for the host galaxy of Type II SN 2004eb (NGC 6387), whose mass-weighted stellar population age is $10^{9.11}(\pm\, 0.39)$ yr, which has a high (95.9%) fraction of young stellar populations. The scatter for the stellar population is too large to give an authentic conclusion and the sample size is insufficient, so we will not give a deep discussion for stellar age.

4.7 Dn(4000) & Hδ_A

Bruzual A. (1983) defined Dn(4000) as the average flux density ratio of the two bands of 4050–4250 and 3750–3950 Å. Later, the average flux density ratio of another two narrower bands, 4000–4100 and 3850–3950 Å, was defined as Dn(4000) by Balogh et al. (1999). The narrower definition has a significant point in that this ratio is less sensitive to reddening effects. In galaxies which experienced a star formation burst that ended about 0.1–1 Gyr ago, a strong Hδ absorption line arose. The peak occurs once hot O and B stars terminated their evolution (Kauffmann et al. 2003b). An Hδ absorption line was defined using a central bandpass bracketed through two pseudo-continuum bandpasses by Worthey & Ottaviani (1997).

As Kauffmann et al. (2003b) pointed out, the depth of the 4000 Å break, Dn(4000), and the equivalent width of the Hδ line, Hδ_A, are rather sensitive indicators of stellar populations that have different ages. Figure 6 displays the distribution of the global Dn(4000) and Hδ_A for our sample galaxies. The lines are taken from Kauffmann et al. (2003a), which present the relations between Dn(4000) and Hδ_A for pure burst star formation histories and for continuous star formation histories with different metallicities. Our sample galaxies are distributed inside the region of the Dn(4000) and H$\delta_{\rm A}$ plane for pure burst and continuous star formation histories with different metallicities. From this figure, there is no significant difference in the global Dn(4000) and Hδ_A for different types of SN galaxies. Table 5 shows that the SN 2004eb host galaxy has the lowest value of global Dn(4000) of 1.2 among our sample host galaxies, which is consistent with the result of stellar population age estimated using `STARLIGHT` in that this galaxy has a larger fraction of young stellar population.

Here the Dn(4000) and Hδ_A of the SN host galaxies in this study are from Li et al. (2015). According to Li et al. (2015), the standard to classify galaxies into centrally quiescent and centrally star-forming is whether the Dn(4000) of the center of the galaxies is larger than 1.6 or not. Among all the 11 SN host galaxies, we can see from Table 5 that the central Dn(4000) of the host galaxies of SN 2007R (PGC 21767), 2000cs (MCG +07-34-015), 2010ee (UGC 8652) and 1975K (NGC 6195) are larger than 1.6, so these galaxies should belong to the centrally quiescent group.

5 DISCUSSION

5.1 Comparing Our Sample with Other Works

Compared with SN host galaxies in Galbany et al. (2016b) from CALIFA, our sample size of SN galaxies from MaNGA is much smaller (132/939 vs. 14/1390). To explore the reason for this, we compare the redshift distributions of these database galaxies observed with CALIFA, MaNGA in SDSS DR13 and SN host galaxies obtained from the catalog in Figure 7. ASC provides redshift information for only 1460 distant galaxies with redshift greater than 0.1. SAI Supernova Catalogue provides redshift information for 5790 galaxies, including 1442 galaxies which are also included in ASC. Therefore, we apply redshift from the SAI Supernova Catalogue for comparison here.

From Figure 7, we can see that there is a peak in the redshift of SN galaxies located at about 0.02 (SAI Supernova Catalogue). Most of the CALIFA DR3 galaxy redshifts range between 0 and 0.03 with a peak of about 0.01. However, the redshifts of galaxies from MaNGA mainly range from 0 to 0.08 with a peak of about 0.03. Therefore, the main reason that our sample size of SN hosts is much smaller than the CALIFA data is due to the different redshift ranges of the sample. MaNGA selects more distant galaxies, among which fewer SN explosions could be observed inside than the much closer ones, such as the CALIFA galaxies.

Also, we check the effect of the diameter of the FoV on different numbers of SNe explored by CALIFA and MaNGA. The largest diameter of the IFU size of MaNGA is 32 arcsec and the FoV of CALIFA is $1.3\,{\rm arcmin}^2$. We obtain 138 SNe by cross-correlating SNe in ASC with 939 galaxies in CALIFA and 23 SNe among 1390 galaxies in MaNGA with the same matching radius of $50''$. Therefore, the smaller sample size of SN galaxies from MaNGA than that from CALIFA is not mainly caused by the smaller FoV of MaNGA.

5.2 Star Formation Rate

Figure 8 shows the distribution of the global SFR and the stellar mass estimated using `STARLIGHT` code. From this figure, most of our sample galaxies are located within or close to the 68% confidence level of the locus of blue SDSS galaxies at $0.015 \leq z \leq 0.1$ in Elbaz et al. (2007) except for host galaxies of SN 2000cs, 2012al and 2004eb. The central region of the host galaxy of SN 2000cs is located in the AGN region, which can be ascertained from Figure 2. According to Table 5, the light-weighted stellar ages of the SNe 2000cs and 2012al host galaxies are older than other galaxies in our sample. The host galaxy of SN 2012al is faint, which can be ascertained from the MaNGA image, and the Hα flux is very low. Thus, for the host galaxies of SN 2000cs and 2012al, the SFRs estimated from Hα flux are much lower than normal star forming galaxies. The host galaxy of SN 2004eb is in an interacting system, which could excite star forming activity and result in a higher SFR than normal galaxies.

5.3 Gas-phase Oxygen Abundance

Figure 9 presents the local gas-phase oxygen abundance at the SN explosion sites and the global gas-phase oxygen abundance of the host galaxies estimated using the O3N2 method. From the figure, we can see that in our sample, SNe Ia tend to explode in galaxies which have higher gas-phase oxygen abundance than SNe II. The gas-phase oxygen abundance of unclassified SN host galaxies is similar

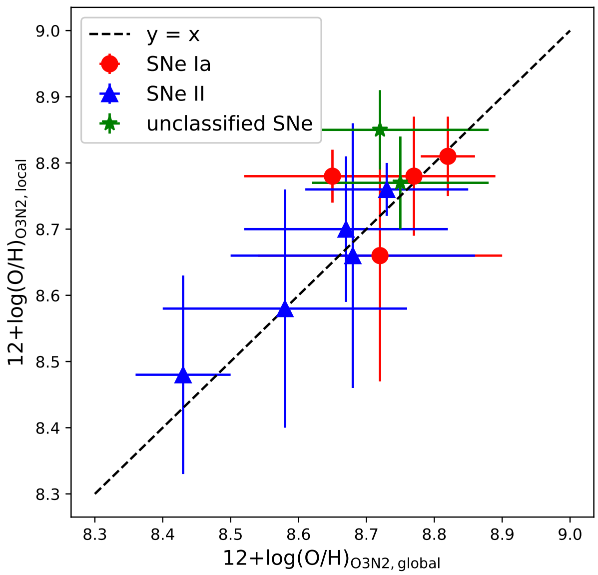

Fig. 9 Diagram of the gas-phase oxygen abundance estimated by the O3N2 method. It reveals the difference between the local gas-phase oxygen abundance of SN explosion sites and that of the global host galaxies for the whole sample. The *red circles*, *blue triangles* and *green stars* represent SNe Ia, SNe II and unclassified types of SNe, respectively.

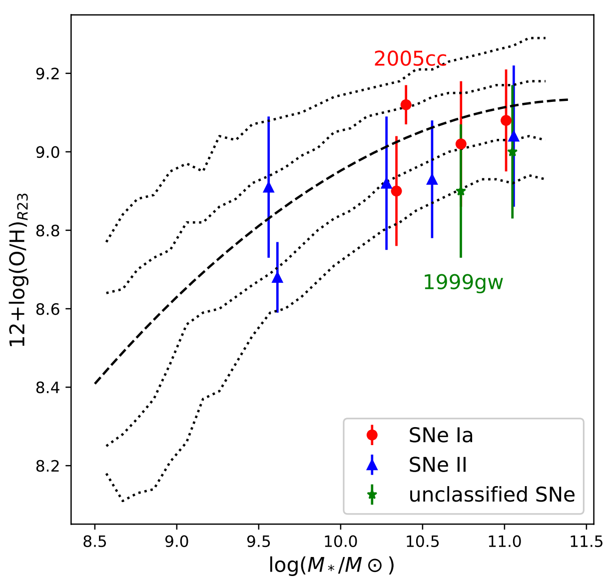

Fig. 10 The distributions of stellar mass and the global gas-phase oxygen abundance of the host galaxies in our sample. Stellar mass is taken from the MaNGA DRP catalog (Law et al. 2016). The gas-phase oxygen abundance is estimated using the R_{23} method. The *dashed line* is the polynomial fitting to the median value in bins of 0.1 dex in mass from Tremonti et al. (2004). The *dotted lines* are the contours that enclose 68% and 95% of the data from Tremonti et al. (2004).

with that of SN Ia host galaxies in our sample. The average local gas-phase oxygen of SNe Ia (12 + log(O/H) $\sim$ 8.76) in the sample host galaxies is also higher than those of SNe II (12 + log(O/H) $\sim$ 8.64). Most of our SN host galaxies are metallicity-richer ones with 12 + log(O/H) $>$ 8.5, except one, the host galaxy of 2004eb (NGC 6387), which has lower oxygen abundance of 8.43.

The dashed line in Figure 9 represents the ratio between global and local gas-phase oxygen abundance of 1:1. This figure demonstrates that most of the SN host galaxies are located near the diagonal line. There is a small difference between the local metallicity at the SNe explosion site and the global metallicity of the host galaxy.

5.4 The Relation Between Stellar Mass and Gas-phase Oxygen Abundance

To compare our SN host galaxies with the SDSS main sample galaxies from Tremonti et al. (2004), we present the distributions of stellar mass described with nsa-mstar in the DRP catalog, which could provide the stellar mass of the whole galaxy (see details in Sect. 4.5), and the global gas-phase oxygen abundance of the host galaxies estimated using the R_{23} method in Figure 10.

In this figure, red dots, blue triangles and green stars represent SNe Ia, SNe II and unclassified SNe, respectively. The dashed line signifies the polynomial fitting to the median value in bins of 0.1 dex in stellar mass from Tremonti et al. (2004). The dotted lines correspond to the contours that enclose 68% and 95% of the data from Tremonti et al. (2004). According to Figure 10, there is a positive relation between stellar mass and metallicity, which is consistent with Tremonti et al. (2004). Most of our sample galaxies are located in the same region as 95% of the data from Tremonti et al. (2004) except for the host galaxy with an unclassified type of SN 1999gw, which is in a merging system. The gas-phase oxygen abundance of the peculiar Type Ia SN 2005cc host galaxy estimated using the R_{23} method is a little higher than those of other sample galaxies. This host galaxy also exhibits the highest gas-phase oxygen abundance estimated using the O3N2 and N2O2 methods.

All the Type Ia SNe in our sample exploded in galaxies with stellar mass higher than $10^{10}\ M_{\odot}$, which is consistent with Galbany et al. (2014). According to Sullivan et al. (2006), SNe Ia also explode in galaxies that have lower mass (than $10^{10}\ M_{\odot}$). The fact that our sample galaxies lack low-mass galaxies may be caused by the small sample size.

6 CONCLUSIONS

In this paper, we analyze the local properties of explosion sites for 11 SNe and global properties of their host galaxies using the IFS of MaNGA.

There are some significant advantages in our work. Compared with multicolor broad-band imaging or integrated spectroscopy, we could derive the 2D maps of parameters for SN galaxies using the spatially resolved spectroscopy of MaNGA to compare the local properties at the SNe explosion sites and the global properties of the SN galaxies. What is more, the higher redshift distribution up to a median of 0.03 allows us to obtain a sample and information about more distant galaxies which host different types of SNe. Thanks to the 2D maps of MaNGA observations, we can analyze these SN host galaxies one by one in great detail including their Hα velocity, sSFR, gas-phase oxygen abundance, stellar population age, etc., for a sample of 11 sample galaxies. The results are summarized as follows.

With the small differences between local metallicity at the SN explosion sites and that of the global galaxy, the metallicity estimated from integrated spectra can represent the local metallicity at SN explosion sites with small bias, which is consistent with Galbany et al. (2016b). Here global refers to the whole area inside the FoV of MaNGA, which covers more than $1.5\,R_e$ or $2.5\,R_e$ of the galaxies. As derived from our sample, SNe tend to explode in metallicity-rich galaxies.

From the velocity field and velocity dispersion map, we can conclude that both SNe Ia and SNe II in our sample could explode in normal galaxies. SNe II also could explode in an interacting or merging system, which has recent star formation. For our sample galaxies, the global and local gas-phase oxygen abundances of SN Ia host galaxies are a little higher than those of SN II host galaxies. On average, the stellar mass of SN Ia host galaxies in our sample is a little higher than that of SN II host galaxies. SNe Ia in our sample could explode in more massive galaxies, but SNe II can explode in both high mass and low mass galaxies. More sample galaxies with lower masses are needed for more information on this topic.

The MaNGA survey will provide a larger sample of SN galaxies, which could give us a firmer statistical conclusion regarding the differences in the explosion environment between different types of SNe, a goal which we will pursue in following work.

Acknowledgements We appreciate the referee who provided very constructive and helpful comments and suggestions, which helped to improve our work very much. We thank Weibin Shi, Wei Du, Hao Tian and Bo Zhang for helpful and significant discussions on this work. We thank Cheng Li, Enci Wang, Ting Xiao and Lin Lin for providing the data on Dn(4000) and Hδ_A, and we thank Yanbin Yang, Francois Hammer and Michel Dennefeld for helpful discussions on kinematics of the galaxies. We thank Zheng Zheng for helpful discussions and comments. This work was supported by the National Natural Science Foundation of China (Grant Nos. 11733006, 11273026, 11233004 and U1631105).

Funding for the Sloan Digital Sky Survey IV has been provided by the Alfred P. Sloan Foundation, the U.S. Department of Energy Office of Science, and the Participating Institutions. SDSS acknowledges support and resources from the Center for High-Performance Computing at the University of Utah. The SDSS web site is `www.sdss.org`.

SDSS is managed by the Astrophysical Research Consortium for the Participating Institutions of the SDSS Collaboration including the Brazilian Participation Group, the Carnegie Institution for Science, Carnegie Mellon University, the Chilean Participation Group, the French Participation Group, Harvard-Smithsonian Center for Astrophysics, Instituto de Astrofísica de Canarias, The Johns Hopkins University, Kavli Institute for the Physics and Mathematics of the Universe (IPMU) / University of Tokyo, the Korean Participation Group, Lawrence Berkeley National Laboratory, Leibniz Institut für Astrophysik Potsdam (AIP), Max-Planck-Institut für Astronomie (MPIA Heidelberg), Max-Planck-Institut für Astrophysik (MPA Garching), Max-Planck-Institut für Extraterrestrische Physik (MPE), National Astronomical Observatories of China, New Mexico State University, New York University, University of Notre Dame, Observatório Nacional / MCTI, The Ohio State University, Pennsylvania State University, Shanghai Astronomical Observatory, United Kingdom Participation Group, Universidad Nacional Autónoma de México, University of Arizona, University of Colorado Boulder, University of Oxford, University of Portsmouth, University of Utah, University of Virginia, University of Washington, University of Wisconsin, Vanderbilt University, and Yale University.

References

Albareti, F. D., Allende Prieto, C., Almeida, A., et al. 2017, ApJS, 233, 25

Alloin, D., Collin-Souffrin, S., Joly, M., & Vigroux, L. 1979, A&A, 78, 200

Arnett, W. D., Bahcall, J. N., Kirshner, R. P., & Woosley, S. E. 1989, ARA&A, 27, 629

Baldwin, J. A., Phillips, M. M., & Terlevich, R. 1981, PASP, 93, 5

Balogh, M. L., Morris, S. L., Yee, H. K. C., Carlberg, R. G., & Ellingson, E. 1999, ApJ, 527, 54

Barbon, R., Ciatti, F., & Rosino, L. 1979, A&A, 72, 287

Barbon, R., Cappellaro, E., Ciatti, F., Turatto, M., & Kowal, C. T. 1984, A&AS, 58, 735

Barbon, R., Cappellaro, E., & Turatto, M. 1989, A&AS, 81, 421
Barbon, R., Buondí, V., Cappellaro, E., & Turatto, M. 1999, A&AS, 139, 531
Becker, S. A., & Iben, Jr., I. 1980, ApJ, 237, 111
Belfiore, F., Maiolino, R., Maraston, C., et al. 2016, MNRAS, 461, 3111
Bethe, H. A., Brown, G. E., Applegate, J., & Lattimer, J. M. 1979, Nuclear Physics A, 324, 487
Blanton, M. R., Bershady, M. A., Abolfathi, B., et al. 2017, AJ, 154, 28
Bruzual A., G. 1983, ApJ, 273, 105
Bruzual, G., & Charlot, S. 2003, MNRAS, 344, 1000
Bundy, K., Bershady, M. A., Law, D. R., et al. 2015, ApJ, 798, 7
Calzetti, D., Armus, L., Bohlin, R. C., et al. 2000, ApJ, 533, 682
Cappellari, M., & Copin, Y. 2003, MNRAS, 342, 345
Chabrier, G. 2003, PASP, 115, 763
Chen, T.-W., Schady, P., Xiao, L., et al. 2017, ApJ, 849, L4
Cid Fernandes, R., Mateus, A., Sodré, L., Stasińska, G., & Gomes, J. M. 2005, MNRAS, 358, 363
Cid Fernandes, R. 2018, MNRAS, 480, 4480
Dobrycheva, D. V. 2013, Odessa Astronomical Publications, 26, 187
Dopita, M. A., Kewley, L. J., Heisler, C. A., & Sutherland, R. S. 2000, ApJ, 542, 224
Dopita, M. A., Sutherland, R. S., Nicholls, D. C., Kewley, L. J., & Vogt, F. P. A. 2013, ApJS, 208, 10
Drory, N., MacDonald, N., Bershady, M. A., et al. 2015, AJ, 149, 77
Elbaz, D., Daddi, E., Le Borgne, D., et al. 2007, A&A, 468, 33
Filippenko, A. V. 1997, ARA&A, 35, 309
Fitzpatrick, E. L. 1999, PASP, 111, 63
Flores, H., Hammer, F., Puech, M., Amram, P., & Balkowski, C. 2006, A&A, 455, 107
Galbany, L., Stanishev, V., Mourão, A. M., et al. 2014, A&A, 572, A38
Galbany, L., Anderson, J. P., Rosales-Ortega, F. F., et al. 2016a, MNRAS, 455, 4087
Galbany, L., Stanishev, V., Mourão, A. M., et al. 2016b, A&A, 591, A48
Galbany, L., Anderson, J. P., Sánchez, S. F., et al. 2018, ApJ, 855, 107
Ge, J.-Q., Hu, C., Wang, J.-M., Bai, J.-M., & Zhang, S. 2012, ApJS, 201, 31
Ge, J., Yan, R., Cappellari, M., et al. 2018, MNRAS, 478, 2633
Hammer, François Puech, M., Flores, H., & Rodrigues, M. 2017, Studying Distant Galaxies: A Handbook of Methods and Analyses (World Scientific Publishing Co. Pte. Ltd.)
Hamuy, M., Maza, J., Pinto, P. A., et al. 2002, AJ, 124, 417
Han, D.-H., Park, C., Choi, Y.-Y., & Park, M.-G. 2010, ApJ, 724, 502
Hoyle, F., & Fowler, W. A. 1960, ApJ, 132, 565
Izotov, Y. I., Stasińska, G., Meynet, G., Guseva, N. G., & Thuan, T. X. 2006, A&A, 448, 955
Izzo, L., Thöne, C. C., García-Benito, R., et al. 2018, A&A, 610, A11
James, P. A., Bretherton, C. F., & Knapen, J. H. 2009, A&A, 501, 207
Kauffmann, G., Heckman, T. M., White, S. D. M., et al. 2003a, MNRAS, 341, 33
Kauffmann, G., Heckman, T. M., Tremonti, C., et al. 2003b, MNRAS, 346, 1055
Kelly, P. L., & Kirshner, R. P. 2012, ApJ, 759, 107
Kennicutt, Jr., R. C. 1998, ARA&A, 36, 189
Kewley, L. J., & Dopita, M. A. 2002, ApJS, 142, 35
Kewley, L. J., Dopita, M. A., Sutherland, R. S., Heisler, C. A., & Trevena, J. 2001, ApJ, 556, 121
Kobulnicky, H. A., & Kewley, L. J. 2004, ApJ, 617, 240
Krajnović, D., Cappellari, M., de Zeeuw, P. T., & Copin, Y. 2006, MNRAS, 366, 787
Kuncarayakti, H., Doi, M., Aldering, G., et al. 2013a, AJ, 146, 30
Kuncarayakti, H., Doi, M., Aldering, G., et al. 2013b, AJ, 146, 31
Kuncarayakti, H., Anderson, J. P., Galbany, L., et al. 2018, A&A, 613, A35
Law, D. R., Yan, R., Bershady, M. A., et al. 2015, AJ, 150, 19
Law, D. R., Cherinka, B., Yan, R., et al. 2016, AJ, 152, 83
Li, C., Wang, E., Lin, L., et al. 2015, ApJ, 804, 125
Liang, Y. C., Yin, S. Y., Hammer, F., et al. 2006, ApJ, 652, 257
Liang, Y. C., Hammer, F., Yin, S. Y., et al. 2007, A&A, 473, 411
Lyman, J. D., Taddia, F., Stritzinger, M. D., et al. 2018, MNRAS, 473, 1359
McGaugh, S. S. 1991, ApJ, 380, 140
Osterbrock, D. E., & Ferland, G. J. 2006, Astrophysics of Gaseous Nebulae and Active Galactic Nuclei (University Science Books)
Pagel, B. E. J., Edmunds, M. G., Blackwell, D. E., Chun, M. S., & Smith, G. 1979, MNRAS, 189, 95
Perlmutter, S., Aldering, G., Goldhaber, G., et al. 1999, ApJ, 517, 565
Pettini, M., & Pagel, B. E. J. 2004, MNRAS, 348, L59
Pilyugin, L. S. 2001, A&A, 374, 412
Pilyugin, L. S., & Thuan, T. X. 2005, ApJ, 631, 231
Prieto, J. L., Stanek, K. Z., & Beacom, J. F. 2008, ApJ, 673, 999
Riess, A. G., Filippenko, A. V., Challis, P., et al. 1998, AJ, 116, 1009
Rubin, A., Gal-Yam, A., De Cia, A., et al. 2016, ApJ, 820, 33
Salim, S., Rich, R. M., Charlot, S., et al. 2007, ApJS, 173, 267
Schlegel, E. M. 1990, MNRAS, 244, 269
Shao, X., Liang, Y. C., Dennefeld, M., et al. 2014, ApJ, 791, 57
Smee, S. A., Gunn, J. E., Uomoto, A., et al. 2013, AJ, 146, 32
Stanishev, V., Rodrigues, M., Mourão, A., & Flores, H. 2012, A&A, 545, A58
Stasińska, G. 2006, A&A, 454, L127
Sullivan, M., Le Borgne, D., Pritchet, C. J., et al. 2006, ApJ, 648, 868

Tremonti, C. A., Heckman, T. M., Kauffmann, G., et al. 2004, ApJ, 613, 898
Turatto, M. 2003, in Lecture Notes in Physics, 598, Supernovae and Gamma-Ray Bursters, ed. K. Weiler, 21 (Berlin Springer Verlag)
Wake, D. 2015, in American Astronomical Society Meeting Abstracts, 225, 143.28
Wake, D. A., Bundy, K., Diamond-Stanic, A. M., et al. 2017, AJ, 154, 86
Weijmans, A.-M., & MaNGA Team. 2016, in ASPC, 507, Multi-Object Spectroscopy in the Next Decade: Big Questions, Large Surveys, and Wide Fields, eds. I. Skillen, M. Balcells, & S. Trager, 257
Worthey, G., & Ottaviani, D. L. 1997, ApJS, 111, 377
Yan, R., Bundy, K., Law, D. R., et al. 2016, AJ, 152, 197
Yang, Y., Flores, H., Hammer, F., et al. 2008, A&A, 477, 789
Zaritsky, D., Kennicutt, Jr., R. C., & Huchra, J. P. 1994, ApJ, 420, 87
Zhang, K., Yan, R., Bundy, K., et al. 2017, MNRAS, 466, 3217